Title

VACUUM FLOW OF GASES THROUGH CHANNELS WITH CIRCULAR, ANNULAR, AND RECTANGULAR CROSS SECTIONS

Author

Dong, Walter.

Publication Date

1956-04-01

Thesis/dissertation

UCRL 3353

UNIVERSITY OF
CALIFORNIA

Radiation Laboratory

VACUUM FLOW OF GASES THROUGH CHANNELS WITH CIRCULAR, ANNULAR, AND RECTANGULAR CROSS SECTIONS

BERKELEY, CALIFORNIA

DISCLAIMER

UCRL-3353
Chemistry Distribution

UNIVERSITY OF CALIFORNIA

Radiation Laboratory
Berkeley, California

Contract No. W-7405-eng-48

VACUUM FLOW OF GASES THROUGH CHANNELS WITH CIRCULAR, ANNULAR, AND RECTANGULAR CROSS SECTIONS

Walter Dong

April 1956

(Thesis)

Printed for the U.S. Atomic Energy Commission

Table of Contents

Tables

VACUUM FLOW OF GASES THROUGH CHANNELS WITH CIRCULAR, ANNULAR, AND RECTANGULAR CROSS SECTIONS

Walter Dong

Radiation Laboratory and
Department of Chemistry and Chemical Engineering
University of California, Berkeley, California

April 1956

Abstract

Vacuum flow of hydrogen, helium, air, carbon dioxide, and Freon-12 was measured in copper channels. These channels included a circular section with a 3.64-cm radius, two annular sections formed by inserting cores of 1.905-cm and 3.174-cm radii into the circular section, respectively, and a rectangular section 0.324 cm by 22.86 cm. In each section the flow was found to approach the molecular-flow limit with decreasing pressure, but the degree of approach depended on the cross section. When the molecular-flow equation was given in terms of the Barrett and Bosanquet geometric factor, K,

$$Q_M = K(4/3)(A^2/0)v(dp/dx) = KQ_A,$$

the degree of approach became poorer as K increased. The data approached the slip-flow limit with increasing pressure in all the channels.

The experimental data were fitted over the entire range with empirical equations of the form

$$Q = Q_L + KQ_A \left[\frac{1 + C_1(X/\lambda)^{C_2}}{1 + C_1 \ 16K/3\pi(X/\lambda)^{C_2}} \right],$$

where Q_L is the laminar flow term, and X/λ the Knudsen number. The data from the rectangular section were fitted with $C_1 = 1.23$ and $C_2 = 0.3$. A general empirical equation for annular and circular sections was obtained when we set $C_1 = 0.275 + 1.27b/a$ and $C_2 = 0.4$.

The fraction of molecules diffusely reflected from copper surfaces was found to decrease with increasing molecular weight. The absolute values of f could not be determined from the data. However, when f = 1 was assumed for hydrogen, the following values of f could be calculated by comparison for the other gases: helium, 0.99; air and carbon dioxide, 0.97; and Freon-12, 0.90.

Equations for slip flow in annular and rectangular sections were derived. Also derived was an approximate slip-flow equation for annular sections that agreed well with the rigorous derivation for channels with ratios of radii greater than 0.5.

A study of the effect of the molecular nature of the gas on slip flow indicated that with decreasing pressure, a positive deviation of flow from the slip-flow equation results. This would explain the apparent decrease in f observed in the slip-flow region.

A simple approximation of the flow in the molecular-flow region was given that consisted of adding to the self-diffusion solution at low Knudsen numbers an additional flow due to streaming. This is expressed by Eq. (2.99).

I. INTRODUCTION AND REVIEW OF THEORY

Although turbulence is usually encountered in the flow of gases at ordinary pressures, it is seldom the nature of the flow in high-vacuum systems. Instead, the mechanism of flow usually lies within the limits of laminar and molecular flows. A determining parameter of the type of flow existing in a vacuum system is the Knudsen number, which is merely the ratio of a characteristic dimension of the system (such as the radius of a tube) to the mean free path of the gas. The flow is laminar when this ratio, X/λ, approaches infinity, and becomes molecular when it goes to zero. Ordinarily, it is adequate to assume laminar flow to exist in a channel when X/λ is greater than 100. Below this value a gradual transition from laminar flow to molecular flow occurs. We can divide this transition region in the following flow regions:

1. $100 > X/\lambda > 10$, slip-flow region;
2. $10 > X/\lambda > 1/10$, transition-flow region;
3. $1/10 > X/\lambda$, molecular-flow region.

Molecular Flow

The molecular-flow equation for infinite cylindrical tubes was originally derived by Knudsen:[20]

$$Q_M = (4/3)v(A^2/0)(dp/dx) , \qquad (1.1)$$

where Q_M = mass flow rate, μ-l/sec,

v = average molecular speed,

A = cross section area of the duct, πa^2 ,

0 = periphery of the duct, $2\pi a$,

and dp/dx = pressure gradient along the duct.

However, it was von Smoluchowski[28] who set out the general molecular-path-tracing method for calculating the rate of flow in any channel. The assumptions made in these calculations were:

1. molecules are reflected from the wall according to the Lambert cosine law.

2. no collisions occur between molecules, and

3. the Maxwellian velocity distribution applies.

Clausing[9-11] evaluated the flow in channels of various cross sections and lengths. The calculations for annular and rectangular sections of infinite length were repeated by Barrett and Bosanquet,[4] and their results agreed with Clausing's. Barrett and Bosanquet also evaluated the flow through an infinitely long channel with an equilateral-triangular cross section. They expressed their results in the form

$$Q_M = Q_A K = \frac{4}{3} \frac{A^2}{0} v \frac{dp}{dx} K ,$$

where K is the geometric factor. It can be seen from Eq. (1.1) that K = 1 for the infinite circular channel.

Laminar Flow

When X/λ approaches infinity, a fluid -- although molecular in nature -- can be considered as a continuum. This condition is satisfied by liquids and by gases at high pressure. If the fluid viscosity is assumed constant and the velocity at the duct wall to be zero, Poisseuille's law can be derived.[22] The equation for laminar flow of gases in annular sections is

$$Q = \frac{\pi}{8\eta} \left[a^4 - b^4 - \frac{(a^2-b^2)^2}{\ln \frac{a}{b}} \right] p \frac{dp}{dx} , \qquad (1.2)$$

where a and b are the outer and inner radii of the annular section, respectively, and η is the viscosity of the gas. When b = 0, this equation reduces to the equation for laminar flow through round tubes. The solution for laminar flow through rectangular sections as derived by Cornish[12] is

$$Q = -\frac{4}{3\eta} a^3 bp \frac{dp}{dx} \left[1 - \frac{192}{\pi^5} \frac{a}{b} \left(\tanh \frac{\pi}{2} \frac{b}{a} + \frac{1}{3^5} \tanh \frac{3\pi}{2} \frac{b}{a} + \frac{1}{5^5} \tanh \frac{5\pi}{2} \frac{b}{a} + \right. \right.$$

$$\left. \left. \cdots\cdots\cdots\cdots\cdots \right) \right] \qquad (1.3)$$

where 2a and 2b are the lengths of the short and long sides of the rectangular section, respectively.

Transition Region

Since any exact treatment of flow in the transition region is inherently very difficult, one usually restricts his attention to the region near the two limits. Prior to Knudsen's vacuum-flow measurements there had been an interest in the slip-flow region because positive deviations from the laminar-flow equation had been observed. To account for the increase in flow, Kundt and Warburg[21] assumed that a finite instead of zero velocity of slip existed at the duct wall. The magnitude of this slip velocity was assumed to be proportional to the velocity gradient at the wall. Using this boundary condition in rederiving Poisseuille's equation, they obtained the equation for flow in tubes,

$$Q = \frac{\pi a^4}{8\eta} p \frac{dp}{dx} \left(1 + 4 \frac{\zeta}{a} \right) , \qquad (1.4)$$

where ζ = coefficient of slip (dimension of length). The first term on the right side of this equation is just that for laminar flow and the second term expresses the additional flow due to slip. By employment of the kinetic theory of gases, it can be shown that when diffuse reflection occurs at the wall, we have

$$\zeta = 2 c \lambda , \qquad (1.5)$$

where c is defined by the expression for viscosity,

$$\eta = c m n v \lambda .$$

In recent years the attention of investigators has been turned to the molecular-flow region. In this region intermolecular collisions cause the flow to deviate from the molecular-flow equation. Pollard and Present[25] calculated the effect of intermolecular collisions on the coefficient of self-diffusion of a gas at uniform pressure in long cylindrical tubes throughout the entire transition region. When a/λ approaches zero their result becomes

$$Q_D = (4/3)v(A^2/0)(dp/dx)\ [\ 1-(1.226 + (3/4)\ \ln\ \lambda/2\gamma_E a)a/\lambda + \ldots\ ]\ , \qquad (1.6)$$

where

γ_E = Euler's constant, 1.781.

As a first approximation this solution can be used to describe the flow in the molecular-flow region.

Pollard and Present indicated that although it was permissible, in the case of self-diffusion, to assume isotropic scattering of molecules after intermolecular collisions, these collisions would impart a streaming velocity to the molecules in the case of flow. Hiby and Pahl[17] estimated this flow by considering the collisions to be related to the single scattering of molecules in a gas with Maxwellian velocity distribution. This resulted in a flow,

$$Q_T = (4/3)v(A^2/0)(dp/dx)\ (1.2a/\lambda), \qquad (1.7)$$

that must be added to the Pollard and Present solution. They suggested the following equation for the flow as a function of Knudsen number,

$$Q = \frac{4}{3}\ \frac{A^2}{0}\ v\ \frac{dp}{dx}\ \left[\ 1 - \frac{3}{4}\ \frac{a}{\lambda}\ \ln\ \frac{\lambda}{2\gamma_E\ a}\ \right] \qquad (1.8)$$

Weber[29] also treated this problem, again by calculating a flow to be added to the Pollard and Present solution. He assumed, a priori, that this flow is constant across the tube, and -- by a momentum balance at the wall --

calculated its magnitude. Weber's solution varies with a/λ and becomes

$$Q_T = (4/3)v(A^2/0)(dp/dx)(\pi a/2\lambda) \qquad (1.9)$$

when a/λ approaches zero. This is the same as Hiby and Pahl's solution except for a factor of $5\pi/12$.

Empirical equations

Workable equations for vacuum flow covering the entire range of X/λ must necessarily be empirical. Knudsen found that an equation of the form

$$Q = \frac{\pi}{8} \frac{a^4}{\eta} p \frac{dp}{dx} \left[1 + \frac{64}{3\pi} \frac{\lambda}{a} \left(\frac{1 + C_1 a/\lambda}{1 + C_2 a/\lambda}\right)\right] \qquad (1.10)$$

can adequately represent his data on flow through glass capillaries, where C_1 and C_2 are adjustable constants. Adzumi[1] employed a simpler equation, of the form

$$Q = \frac{\pi}{8} \frac{a^4}{\eta} p \frac{dp}{dx} \left[1 + \gamma \frac{64}{3\pi} \frac{\lambda}{a}\right] ,$$

but the quantity γ must be known as a function of λ/a.

Flow measurements

A large amount of data is available for the flow of gases through long tubes. To mention a few works, Knudsen,[20] Gaede,[15] Adzumi,[1] Todd,[27] and others made flow measurements in glass capillaries; Cheng[7,10] measured the flow of air and hydrogen in copper tubes and of air in iron pipes; and Alancraig[2,3] measured the flow of air in a copper tube. With the exception of the data on iron pipes, where the rough inner surfaces probably affected the flow, and some tubes where systematic errors were obvious, the data closely approached the molecular-flow limit at low pressures, but were consistently higher than the flow given by the slip-flow equation in the slip-flow region. This deviation at large a/λ has often been explained by the assumption that the fraction of molecules diffusely reflected is less than one.

Flow data from channels with other cross sections are rather meager, and these data are inconsistent with each other. Gaede measured the flow of hydrogen in a rectangular glass channel; Rasmussen[26] measured the flow of hydrogen and carbon dioxide in an annular glass channel and hydrogen in a rectangular glass channel; and Alancraig measured the flow of air in four annular copper sections.

Fraction of molecules diffusely reflected

In the discussion above the assumption was made that all molecules were diffusely reflected from the wall. However, this may not necessarily be true in the actual case, and some specular reflection occurs. Maxwell[23] showed that the coefficient of slip must be multiplied by a factor $(\frac{2}{f} - 1)$ when only a fraction f of the molecules was diffusely reflected from the wall. For the same reasoning the molecular flow equation must also be multiplied by this factor to account for any specular reflection.

The f's calculated from molecular-flow data in tubes are usually quite close to 1. On the other hand, slip-flow data in the same tubes yield a value of approximately 0.9 for f if we assume the slip-flow equation to be valid.

Objectives of this work

Since conflicting results were obtained in vacuum-flow measurements in annular and rectangular channels by previous workers, additional flow measurements are desirable so that this disagreement may be clarified. Accordingly, flow is measured in a circular, a rectangular, and two annular sections. The same material, copper, is used for each channel.

It has usually been believed that the fraction of molecules diffusely reflected was independent of the gas even though it was known to be dependent upon the surface. To see if copper surface affects the reflection of different

gases, the flows of hydrogen, helium, air, carbon dioxide, and Freon-12 are measured. This represents a range of molecular weight of from 2 to 121.

Slip-flow equations for annular section and rectangular sections are derived. The deviation of flow from the slip-flow and molecular flow equations in the respective flow regions is studied.

II. THEORY

Slip Flow

Annular Section

The solution of the Navier-Stokes equation for the velocity distribution in an annular section[22] is

$$u = \frac{1}{4\eta} \frac{dp}{dx} r^2 + C_1 \ln r + C_2, \qquad (2.1)$$

where

η = viscosity ,

$\frac{dp}{dx}$ = pressure gradient in the flow direction,

r = radius,

and C_1, C_2 = constants determined by the boundary conditions.

For convenience, we shall write $Y = \frac{1}{4\eta} \frac{dp}{dx}$.

When the boundary conditions are

$$\text{at } r = a,\ u = 0,$$

$$\text{and at } r = b,\ u = 0,$$

where a and b are the radii of the outer and inner tubes, respectively, we get the equation for the laminar-flow velocity distribution,

$$u = Y \left[(r^2 - a^2) - \frac{(a^2 - b^2)}{\ln \frac{a}{b}} \ln \frac{r}{a} \right]$$

The flow rate is obtained by integrating across the channel,

$$Q = p \int_b^a u \cdot 2\pi r dr . \qquad (2.2)$$

This gives us

$$Q = - \frac{\pi a^4 Z}{8\eta} p \frac{dp}{dx} , \qquad (2.3)$$

where

$$Z = 1 - k^4 + \frac{(1-k^2)^2}{\ln k}$$

and

$$k = \frac{b}{a} \quad .$$

The equation for slip flow is obtained by introducing the boundary conditions

$$\text{at } r = a, \qquad \tau_a = \epsilon\, u_{oa} = -\eta\left(\frac{du}{dr}\right)_a , \tag{2.4}$$

and

$$\text{at } r = b, \qquad \tau_b = \epsilon\, u_{ob} = \eta\left(\frac{du}{dr}\right)_b , \tag{2.5}$$

where τ_a and τ_b are the shear stresses at the wall of the outer and inner tube, respectively, and ϵ is the external coefficient of friction. Eqs. (2.4) and (2.5) can be rewritten

$$u_{oa} = -\zeta\left(\frac{du}{dr}\right)_a \tag{2.6}$$

and

$$u_{ob} = \zeta\left(\frac{du}{dr}\right)_b , \tag{2.7}$$

where ζ is the coefficient of slip. When Eq. (2.1) and its differentiation with respect to r are introduced into Eqs. (2.6) and (2.7), we get

$$Ya^2 + C_1 \ln a + C_2 = -\zeta\left(2Ya + \frac{C_1}{a}\right) \tag{2.8}$$

and

$$Yb^2 + C_1 \ln b + C_2 = \zeta\left(2Yb + \frac{C_1}{b}\right) . \tag{2.9}$$

The term C_2 is eliminated from Eqs. (2.7) and (2.8), giving us

$$C_1 = -\frac{Y\,[2\zeta(a+b) + (a^2-b^2)]}{\ln\frac{a}{b} + \zeta\left(\frac{1}{a} + \frac{1}{b}\right)} \quad .$$

Now, by subtracting Eq. (2.8) from Eq. (2.1), we get the equation for the slip-flow velocity distribution,

$$u = Y\,(r^2 - a^2) + C_1 \ln \frac{r}{a} - \zeta\left(2Ya + \frac{C_1}{a}\right) . \qquad (2.10)$$

The total flow rate is obtained, as before, by integrating according to Eq. (2.2). The result of this integration is

$$Q = -\frac{\pi}{2\eta}\, a^4\, p\, \frac{dp}{dx}\left(\frac{1}{\ln \frac{1}{k} + \frac{\zeta(1+k)}{a\ k}}\right)\left(\frac{Z^4}{4} \ln \frac{1}{k} + D_1 \frac{\zeta}{a} + D_2 \frac{\zeta^2}{a^2}\right), \qquad (2.11)$$

where

$$D_1 = \frac{(1-k)(1-k^4)}{4\ k} - \frac{(1-k^2)(1+k)}{2} - (1+k^3) \ln k$$

and

$$D_2 = \frac{(1-k^4)}{k} .$$

It is obvious that this equation is too unwieldy for general use; therefore a simpler approximate solution is desirable. By defining an average velocity of slip that is the same at both walls, we can reduce the slip-flow equation to the sum of a laminar-flow and a slip-flow term. A logical average velocity of slip, $u_{o\ avg}$, is one defined so as to retain the over-all momentum balance at the walls as follows:

$$\tau_{avg}(2\pi a + 2\pi b)\, dx = \tau_a(2\pi a)\, dx + \tau_b(2\pi b)\, dx$$

or

$$\epsilon\, u_{o\ avg}(2\pi a + 2\pi b)\, dx = \epsilon\, u_{oa}(2\pi a)\, dx + \epsilon\, u_{ob}(2\pi b)\, dx. \qquad (2.12)$$

Simplifying Eq. (2.12), we get

$$u_{o\ avg} = \frac{a}{a+b}\ u_{oa} + \frac{b}{a+b}\ u_{ob} . \qquad (2.13)$$

When Eqs. (2.1), (2.6), and (2.7) are substituted into Eq. (2.13) the average slip velocity becomes

$$u_{o\ avg} = -2\,Y\ \zeta(a-b) . \qquad (2.14)$$

The slip term is

$$Q_s = u_{o\ avg}\ A\ p \tag{2.15}$$

where A is the cross section of the channel. Eq. (2.15) becomes

$$Q_s = -\frac{p\zeta}{2\eta}\ \frac{dp}{dx}\ (a-b)\ A \tag{2.16}$$

when Eq. (2.14) is introduced. Eq. (2.16) can also be written

$$Q_s = -\zeta\frac{p}{\eta}\ \frac{dp}{dx}\ \frac{A^2}{O}\ , \tag{2.16a}$$

where O is the periphery of the channel. The total flow rate is obtained by adding Eq. (2.16a) to Eq. (2.2):

$$Q = -\frac{\pi a^4 Z}{8\eta}\ p\ \frac{dp}{dx} - \zeta\frac{A^2}{O}\ p\ \frac{dp}{dx}\ . \tag{2.17}$$

Equation (2.17) can be rewritten

$$Q = -\frac{\pi a^4 Z}{8\eta}\ p\ \frac{dp}{dx}\ \left(1 + 4\ \frac{\zeta}{X}\right)\ , \tag{2.17a}$$

where

$$X = \frac{a(1+k)Z}{(1-k^2)^2}\ . \tag{2.18}$$

This equation becomes rigorous when k = 0. At other values of k, a comparison of the approximate solution, Eq. (2.17), with the rigorous solution, Eq. (2.11), is shown in Table I, where the ratios of the flows calculated from Eq. (2.17) to that calculated from Eq. (2.11) are tabulated for several values of k.

Table I

Ratio of flows calculated with Eqs. (2.17) and (2.11) as a function of k and $\frac{a}{\zeta}$

$\frac{a}{\zeta}$	Q(2.17)/Q(2.11)				
	k = 0.01, $\frac{X}{a}$ = 0.7831	k = 0.1, $\frac{X}{a}$ = 0.6445	k = 0.2, $\frac{X}{a}$ = 0.4805	k = 0.5, $\frac{X}{a}$ = 0.2800	k = 0.75, $\frac{X}{a}$ = 0.1484
1000	0.9951	0.9989	0.9995	0.9998	1.0000
100	0.9624	0.9904	0.9951	0.9986	0.9996
10	0.9056	0.9570	0.9773	0.9949	0.9991

Rectangular Section

A series solution for laminar flow in rectangular sections was given by Cornish.[12] It is possible to extend Cornish's solution to cover the case of slip flow. The hydrodynamics equation for this case are

$$\frac{\partial p}{\partial x} = \eta \left(\frac{\partial^2 u}{\partial z^2} + \frac{\partial^2 u}{\partial y^2} \right), \tag{2.19}$$

$$\frac{\partial p}{\partial z} = 0 , \tag{2.20}$$

$$\frac{\partial p}{\partial y} = 0 , \tag{2.21}$$

$$v = 0,$$

and $$w = 0,$$

where $u = u(z,y)$,

x = direction of flow,

y = direction parallel to short side of the cross section,

and z = direction parallel to long side of the cross section.

The boundary conditions for slip flow are,

$$\text{at} \quad z = \pm b , \qquad u \Big|_{\pm b, y} = \mp \zeta \frac{\partial u}{\partial z} \Big|_{\pm b, y} , \tag{2.22}$$

$$\text{and} \quad y = \pm a , \qquad u \Big|_{z, \pm a} = \mp \zeta \frac{\partial u}{\partial y} \Big|_{z, \pm a} . \tag{2.23}$$

Let $$u = \chi + E\,(a^2 - y^2 + 2a\zeta), \tag{2.24}$$

where $$E = -\frac{1}{2\eta} \frac{dp}{dx} \tag{2.25}$$

and $\chi = \chi(z,y)$.

Substituting Eq. (2.24) into Eq. (2.19), we get

$$\frac{\partial^2 \chi}{\partial z^2} + \frac{\partial^2 \chi}{\partial y^2} = 0 \qquad (2.26)$$

Now let us assume that

$$\chi = Z(z)Y(z), \qquad (2.27)$$

where Z(z) is a function of z only and Y(y) is a function of y only. Substituting Eq. (2.27) into Eq. (2.26) and rearranging, we get

$$\frac{1}{Z} \frac{\partial^2 Z}{\partial z^2} = -\frac{1}{Y} \frac{\partial^2 Y}{\partial y^2} \qquad (2.28)$$

The left side of Eq. (2.28) is a function of z only and the right side, a function of y only; therefore both terms are constant. Let

$$\frac{1}{Z} \frac{d^2 Z}{dz^2} = q^2 \qquad (2.29)$$

and

$$\frac{1}{Y} \frac{d^2 Y}{dy^2} = -q^2 , \qquad (2.30)$$

where q^2 is a constant. The solutions of Eqs. (2.29) and (2.30) are

$$Z = C_1 \sinh qz + C_2 \cosh qz \qquad (2.31)$$

and

$$Y = C_3 \sin qy + C_4 \cos qy , \qquad (2.32)$$

where C_1, C_2, C_3, and C_4 are constants of integration. Since it is obvious that Z and Y are even functions, C_1 and C_3 are zero, and we get

$$\chi = C \cosh qz \cos qy, \qquad (2.33)$$

where

$$C = C_2 C_4 .$$

Eq. (2.24) becomes

$$\chi \Big|_{z,a} = -\zeta \frac{\partial \chi}{\partial y} \Big|_{z,a} \qquad (2.34)$$

when we apply boundary condition Eq. (2.23) at y = a. Substituting Eq. (2.33) into Eq. (2.34) we get

$$\left(\frac{\zeta}{a}\right) qa = \cot qa \ . \tag{2.35}$$

Using the roots of Eq. (2.35), q_j's, we get a series solution,

$$\chi = \sum_{j=1}^{\infty} C_j \cosh q_j z \cos q_j y. \tag{2.36}$$

Now we introduce the second boundary condition Eq. (2.22) to Eq. (2.24), giving us

$$\sum_{j=1}^{\infty} C_j \cos q_j y(\cosh q_j b + \zeta q_j \sinh q_j b) = E(y^2 - a^2 - 2a\zeta). \tag{2.37}$$

Making use of the orthogonality of the eigenfunctions, we evaluate the C_j's with the equation

$$C_j = \frac{\int_{-a}^{a} E(y^2 - a^2 - 2a\zeta) \cos q_j y \, dy}{W_j \int_{-a}^{a} \cos^2 q_j y \, dy} , \tag{2.38}$$

where

$$W_j = \cosh q_j b + \zeta q_j \sinh q_j b.$$

The integration of Eq. (2.38) yields

$$C_j = - \frac{4 E \sin q_j a}{q_j^2 W_j (q_j a + \sin q_j a \cos q_j a)} \ . \tag{2.39}$$

From Eqs. (2.24), (2.36), and (2.39) we get the velocity distribution,

$$u = E(a^2 - 2a\zeta - y^2) - \sum_{j=1}^{\infty} \frac{4E \sin q_j a \cosh q_j z \cos q_j y}{q_j^2 W_j (q_j a + \sin q_j a \cos q_j a)} \ . \tag{2.40}$$

The flow rate is obtained by integrating across the channel:

$$Q = p \int_{-a}^{a} \int_{-b}^{b} u \, dz \, dy \ . \tag{2.41}$$

By a straightforward integration of Eq. (2.41) we obtain the result for slip flow in rectangular sections:

$$Q = -\frac{4}{3}\frac{a^3 b}{\eta} p \frac{dp}{dx}\left[1 + \frac{3\zeta}{a} - \frac{6a}{b}\sum_{j=1}^{\infty} \frac{\sin q_j a \sinh q_j b}{(q_j a)^4 W_j (q_j a + \sin q_j a \cos q_j a)}\right]. \tag{2.42}$$

Some limiting cases of Eq. (2.42) are:

(a) When $\frac{\zeta}{a} = 0$, the roots of Eq. (2.35) become

$$q_j = \frac{(2j-1)}{2a}\pi \qquad j = 1, 2, \ldots .$$

and Eq. (2.42) reduces to Cornish's solution,

$$Q = Q_{L,\infty}\left[1 - \frac{192a}{\pi^5 b}\sum_{j=1}^{\infty}\left(\frac{1}{2j-1}\right)^5 \tanh\frac{b}{a}\frac{(2j-1)}{2}\pi\right], \tag{2.43}$$

where $Q_{L,\infty} = -\frac{4}{3}\frac{a^3 b}{\eta} p \frac{dp}{dx}$. (2.44)

(b) When $\frac{a}{b} = 0$, Eq. (2.42) reduces to the slip-flow equation for flow between infinite parallel plates,

$$Q = Q_{L,\infty}\left(1 + \frac{3\zeta}{a}\right). \tag{2.45}$$

(c) When $\frac{\zeta}{a} \longrightarrow 0$,

$$Q = Q_{L,\infty}\left[1 + \frac{3\zeta}{a} - \frac{6a}{b}\sum_{j=1}^{\infty}\frac{1}{(q_j a)^5 (\coth q_j b + (\frac{\zeta}{a}) q_j a)}\right]. \tag{2.46}$$

(d) When $\frac{b}{a} \longrightarrow 0$,

$$Q = Q_{L,\infty}\left[1 + \frac{3\zeta}{a} - \frac{6a}{b}\sum_{j=1}^{\infty}\frac{\sin q_j a}{(q_j a)^4 (q_j a + \sin q_j a \cos q_j a)(1 + \frac{\zeta}{a}(q_j a))}\right]. \tag{2.47}$$

(e) When $\frac{a}{b} \longrightarrow 0$ and $\frac{\zeta}{a} \longrightarrow 0$,

$$Q = Q_{L,\infty} \left[1 + \frac{3\zeta}{a} - \frac{6a}{b} \sum_{j=1}^{\infty} \frac{1}{(q_j a)^5 \left(1 + \frac{\zeta}{a}(q_j a)\right)} \right]. \qquad (2.48)$$

When the aspect ratio is large the flow can be given by the approximate equation,

$$Q = Q_{L,\infty} \left(\phi + \frac{3\zeta}{a} \right), \qquad (2.49)$$

where ϕ is the term in the bracket in Eq. (2.43).

Breaking Down of the Slip-Flow Equation

In the derivation of the slip-flow equations the gas was assumed to be a continuum. Now we want to study the effect of the molecular nature of the gas on slip flow. Only the flow between infinite parallel plates is considered. The molecular model from classical kinetic theory is used to treat this problem. The assumptions are:

(a) the streaming velocity is so small compared with the molecular velocity that it does not affect the Maxwellian velocity distribution appreciably;

(b) molecules carry with them the property corresponding to the last point of collision; and

(c) molecules are diffusely reflected from the wall.

Whatever the bulk velocity distribution may be in the channel, it must satisfy the condition that the shear stress on any plane parallel to the wall is proportional to the distance of the plane from the center of the duct. This can be stated mathematically as

$$\tau = \frac{y}{a} \quad \tau_W ,$$

where y = perpendicular distance from the duct center to a plane parallel to the wall,

a = distance from the duct center to the duct wall,

τ = shear stress on a plane at a distance y from the center,

and τ_W = shear stress on the duct wall.

In the following discussion the momentum transfer that accompanies diffusion is first neglected and then considered separately later, since its contribution to the total momentum transfer is small in the slip-flow region. According to the slip-flow derivation, the velocity distribution is parabolic with a finite slip velocity at the wall. If this velocity distribution were correct, the shear stress calculated from it would satisfy Eq. (2.50).

Let us consider the momentum carried by molecules crossing an element of area dS in the plane S as shown in Fig. 25. A molecule crossing dS originates from either the wall or some point in the gas following a collision with another molecule. Let us consider the momentum transfer by the latter process. The number of molecules colliding per unit time in an element of volume dV is

$$\frac{nv}{\lambda} \quad dV \quad ,$$

where n = molecular concentration in dV,

v = average molecular speed,

and λ = mean free path.

The fraction of these molecules leaving in the direction toward dS is $d\omega/4\pi$, where $d\omega$ is the solid angle subtended by dS at dV. The probability of a molecule's reaching dS without suffering another collision is $e^{-\rho/\lambda}$, where ρ is the distance between dV and dS. The momentum carried by each molecule across dS relative to the momentum at dS is

$$m\,(u - u_S) \ ,$$

where m = molecular mass,

u = bulk velocity at dV,

and u_S = bulk velocity at dS.

Thus the equation for the rate of momentum transfer across dS from dV relative to dS is

$$dM_{Sb} = \frac{nv}{\lambda} \ dV \quad \frac{d\omega}{4\pi} \ m\,(u - u_S) \ e^{-\rho/\lambda} \ . \qquad (2.51)$$

We now make the following substitutions into Eq. (2.51):

$$\rho = \frac{W}{\cos \alpha} \qquad (2.52)$$

$$d\omega = \frac{dS \sin \alpha}{\rho^2} \qquad (2.53)$$

and $$dV = \rho^2 \, d\rho \sin \alpha \, d\alpha \, d\Theta . \qquad (2.54)$$

Eq. (2.45) becomes

$$dM_{Sb} = \frac{mv}{4\pi} dS \quad e^{-W/\lambda\cos\alpha} \sin\alpha \, d\alpha d\theta \quad n(u - u_S) \, d\left(\frac{W}{\lambda}\right). \tag{2.55}$$

The rate of momentum transfer from the wall across dS relative to dS is obtained in much the same way as for dM_{Sb}. The rate at which molecules leave dS' in the direction toward dS is

$$\frac{nv \, d\omega_S}{4\pi} \, dS' \, ,$$

where $d\omega_S$ is the solid angle subtended by dS at dS'. The momentum carried by each molecule relative to the momentum at dS is $(-mu_S)$. Thus we get

$$dM_{SW} = nv \quad \frac{d\omega_S}{4\pi} \quad dS' \, e^{-\rho_S/\lambda} \quad (-mu_S) \, . \tag{2.56}$$

When

$$dS' = \rho_S^2 \quad \frac{\sin\alpha}{\cos\alpha} \quad d\alpha \, d\theta \tag{2.57}$$

and Eqs. (2.52) and (2.53) are substituted into Eq. (2.56) we get

$$dM_{SW} = -\frac{mv}{4\pi} d\,S \, e^{-W_S/\lambda\cos\alpha} \sin\alpha \cos\alpha \, d\alpha \, d\theta \, n \, u_S \, . \tag{2.58}$$

The quantities u, u_S, n, and λ in Eqs. (2.55) and (2.58) are pressure-dependent, but it is difficult to take this into account rigorously. The function $e^{-\rho/\lambda}$ decreases very rapidly with ρ/λ; therefore the molecules having the most effect on the momentum transfer at dS come from the region near dS. If in addition the pressure gradient is small compared to the total pressure, we can assume λ to be constant and characteristic of the pressure at dS. As a first approximation we can also assume the product nu to be constant along the duct, making it a function of y only.

The equations for the parabolic velocity distribution in terms of W and W' (in the region $-a < y < a$) are:

$$u' = u_o + \left[1 - \frac{(a - W' - W_S)^2}{a^2} \right] (u_m - u_o), \qquad (2.59)$$

$$u = u_o + \left[1 - \frac{(a + W - W_S)^2}{a^2} \right] (u_m - u_o), \qquad (2.60)$$

and

$$u_S = u_o + \left[\frac{2 a W_S - W_S^2}{a^2} \right] (u_m - u_o). \qquad (2.61)$$

To avoid confusion it is well to state now that a, W, W', and W_S are always positive quantities.

For the moment let us consider the momentum transfer at the wall in the case where a/λ is large. Under this condition M_{SW} is small and can be neglected. If we let

$$\gamma_a = \frac{a}{\lambda}, \ \gamma_S = \frac{W_S}{\lambda}, \ \gamma = \frac{W}{\lambda}, \text{ and } \gamma' = \frac{W'}{\lambda} \qquad (2.62)$$

in Eqs. (2.60) and (2.61), the rate of momentum transfer from the gas to the upper plate, Eq. (2.55) is

$$\int dM_b = C \int_0^{2\gamma_a} e^{-\gamma/\cos\alpha} \left[\frac{u_o \gamma_a^2}{(u_m - u_o)} + 2\gamma - \gamma^2 \right] d\gamma , \qquad (2.63)$$

where $$C = \int_0^{\frac{\pi}{2}} \frac{mV}{4\pi} \, dS \sin\alpha \, d\alpha \, \frac{n(u_m - u_o)}{\gamma^2} \int_0^{2\pi} d\Theta , \qquad (2.64)$$

and $u_S = 0$.

Since the exponential term decreases very rapidly as γ increases, we can integrate Eq. (2.63) from zero to infinity. The result of the integration is

$$M_b = C \left[\frac{u_o \gamma_a^2}{u_m - u_o} \cos\alpha + (2\gamma_a - 2\cos\alpha) \cos^2\alpha \right] . \qquad (2.65)$$

Integrating Eq. (2.59) with respect to α, we get

$$M_b = \frac{mnv}{2} \, dS \left[\frac{u_o}{2} + (u_m - u_o)\left(\frac{2}{3\gamma_a} - \frac{1}{2\gamma_a^2}\right) \right] . \tag{2.66}$$

The term in the bracket of Eq. (2.66) is one-half the average velocity of the molecules arriving at the wall; therefore it is equal to u_o, the slip velocity. Thus, we get

$$u_o = (u_m - u_o)\left(\frac{4}{3\gamma_a} - \frac{1}{\gamma_a^2}\right) . \tag{2.67}$$

When $\gamma_a \longrightarrow > \infty$, Eq. (2.66) becomes

$$u_{o,\infty} = (u_m - u_{o,\infty}) \frac{4}{3\gamma_a} \tag{2.68}$$

Now we can rewrite Eq. (2.67):

$$u_o = u_{o,\infty} \left(1 - \frac{3}{4\gamma_a}\right) \tag{2.69}$$

The slip-flow assumption for the velocity of slip is

$$u_{os} = \left(\frac{du}{dW}\right)_{Wall}.$$

The coefficient of slip with f = 1 is given by Eq. (1.5). If we substitute the kinetic-theory value of c = 1/3 into Eq. (1.5), we get, for the velocity of slip,

$$u_{os} = \frac{2}{3} \lambda \left(\frac{du}{dW}\right)_{Wall}. \tag{2.70}$$

The term $\left(\frac{du}{dW}\right)_{Wall}$ can be evaulated from Eq. (2.60) to give us

$$u_{os} = (u_m - u_{os}) \frac{4}{3\gamma_a} = u_{o,\infty} . \tag{2.71}$$

This shows that the velocity of slip in the slip-flow derivation is valid only when the γ_a is very large.

The calculation of the shear stress distribution across the duct, starting with Eqs. (2.55) and (2.58) and assuming the parabolic velocity distribution, is given in the Appendix. The results obtained for $\gamma_a = 5$ and $\gamma_a = 10$ are tabulated in Table II. Column 1 gives the position in the duct. Column 2 shows the values of M_S/B calculated from Eq. (A.12), where

$$B = \frac{mnv}{2\gamma_a 2} \quad dS \ (u_m - u_o).$$

Column 3 shows the true values of M/B, which satisfy Eq. (2.50). The ratios of the values in Column 2 to those in Column 3 are tabulated in Column 4. These calculations indicate that the parabolic velocity distribution gives a rate of momentum transfer that is too low, especially near the wall. However, the momentum transfer due to diffusion may be sufficient to balance the discrepancy.

Table II

Comparison of shear stresses calculated from a parabolic velocity distribution with the true shear stresses

(1) $\frac{y}{a}$	(2) $\left(\frac{M_S}{B}\right)_{calc}$	(3) $\left(\frac{M}{B}\right)_{true}$	(4) $\frac{M_S}{M}$
	$\gamma_a = 10$	$(\frac{X}{\lambda} = 20)$	
0	12.333	13.333	0.925
0.1	11.491	12.0	0.958
0.5	6.660	6.667	0.999
1.0	0	0	1.00
	$\gamma_a = 5$	$(\frac{X}{\lambda} = 10)$	
0	5.665	6.667	0.850
.1	5.343	6.0	0.890
.5	3.280	3.333	0.984
1.0	0	0	1.00

Momentum Transfer due to Diffusion

In the discussion above, the momentum transfer due to diffusion was neglected. Let us consider the expression for the rate of momentum transfer from dV across dS again, this time taking it into account. We may refer to Fig. 25 again. The collision rate of molecules with molecular speed ν in dV is

$$\frac{n \ f(\nu) \ d\nu}{\lambda} \ . \tag{2.72}$$

The total momentum carried by each of these molecules relative to the momentum at dS is

$$m(u - u_S - \nu \cos \Theta \sin \alpha).$$

The equation for dM_b is then

$$dM_b = \frac{(n\nu \ f(\nu) \ d\nu)}{\lambda} \ dV \ \frac{d\omega}{4\pi} \ m \ (u - u_S - \nu \cos \Theta \sin \alpha) \ e^{-\rho/\lambda} \ . \tag{2.73}$$

Eq. (2.73) can be separated into two parts:

$$dM_b = \left(\frac{n\nu \ f(\nu) \ d\nu}{\lambda} \right) dV \ \frac{d\omega}{4\pi} \ m \ (u - u_S) \ e^{-\rho/\lambda}$$

$$- \left(\frac{n\nu \ f(\nu) \ d\nu}{\lambda}\right) dV \ \frac{d\omega}{4\pi} \ m\nu \ \cos \Theta \ \sin \alpha \ e^{-\rho/\lambda} \ . \tag{2.74}$$

When Eq. (2.74) is integrated with respect to ν we get

$$dM_b = \left(\frac{nv}{\lambda}\right) dV \ \frac{d\omega}{4\pi} \ m \ (u - u_S) \ e^{-\rho/\lambda}$$

$$- \left(\frac{n\overline{v^2}}{\lambda}\right) dV \ \frac{d\omega}{4\pi} \ m \cos \Theta \sin \alpha \ e^{-\rho/\lambda} \ , \tag{2.75}$$

or

$$dM_b = dM_{Sb} + dM_{Db} \ . \tag{2.75a}$$

Equation (2.75) states that to account for the rate of momentum transfer by diffusion, M_{Db}, all that is necessary is to add M_{Db} to the previous result obtained by neglecting it. The corresponding term for the momentum transfer due to diffusion from molecules leaving the wall across dS can be obtained

in a similar fashion, but it is not needed in the following treatment.

We shall calculate M_D to the wall. When γ_a is large, $M_D \cong M_{Db}$. If we let plane S be the top plate in Fig. 25 and substitute Eqs. (2.60) and (2.61) into the second term of Eq. (2.75), we get

$$dM_D = -n \overline{v^2} \frac{m}{4\pi} dS \cdot \cos\Theta \, d\Theta \cos\alpha \sin^2\alpha \, d\alpha \, e^{-\rho/\lambda} \, d\frac{\rho}{\lambda} . \qquad (2.76)$$

Again, when γ_a is large, we can integrate ρ/λ from 0 to ∞. We account for the variations of n in the x direction with the equation

$$n = n_o + x \frac{dn}{dx} = n_o + \rho \cos\Theta \sin\alpha \frac{dn}{dx} . \qquad (2.77)$$

When Eq. (2.77) is introduced into Eq. (2.76), the term involving n_o will vanish upon integration owing to symmetry. The integral form of Eq. (2.76) becomes

$$\int dM_D = -\frac{m\overline{v^2}}{4\pi} dS \frac{dn}{dx} \int_0^{2\pi} \cos^2\Theta \, d\Theta \int_0^{\frac{\pi}{2}} \cos\alpha \sin^3\alpha \, d\alpha \int_0^{\infty} e^{-\rho/\lambda} \, d\frac{\rho}{\lambda} , \qquad (2.78)$$

or, when integrated,

$$M_D = -\frac{m\overline{v^2}}{16} \lambda \frac{dn}{dx} dS . \qquad (2.79)$$

Substituting

$$\overline{v^2} = \frac{3p}{mn}$$

into Eq. (2.79), we get

$$M_D = -\frac{3}{16} \lambda \frac{dp}{dx} dS . \qquad (2.80)$$

The fraction of the total momentum transfer due to M_D is

$$\frac{M_D}{M} = \frac{-\frac{3}{16} \lambda \frac{dp}{dx} 0 \, dx}{-A \frac{dp}{dx} dx} = \frac{3}{16 \gamma_a} . \qquad (2.81)$$

For γ_a = 10 and 5, the fractions are 0.0188 and 0.0375 respectively. When these values are added to the values in column 4 of Table II for $\frac{y}{a} = 0$

the results are only 0.944 and 0.888 respectively; therefore the diffusion momentum transfer does not account for the entire discrepancy.

In order to attain the correct rate of momentum transfer in the duct, the velocity gradient near the wall and the slip velocity must increase. The slip velocity necessary to balance the shear stress at the wall can easily be obtained if M_D is taken to be correct.

We know that we have

$$M = M_S' + M_D \tag{2.82}$$

and

$$M_S' = \frac{nv}{2} dS\ m\ u_o' , \tag{2.83}$$

where M_S' is the correct rate of momentum transfer due to bulk movement of the gas and u_o' is the slip velocity necessary to give M_S'. Equation (2.82) can be rewritten

$$M_S' = M\left(1 - \frac{3}{16\gamma_a}\right) , \tag{2.84}$$

when Eq. (2.81) is substituted, and can be reduced to

$$u_o' = u_{o,\infty}\left(1 - \frac{3}{16\gamma_a}\right) . \tag{2.85}$$

Although it is possible to calculate the velocity distribution across the duct as a function of γ_a, such calculations are not warranted, in view of the simplifying assumptions made in this section.

Qualitatively, the results obtained can be used to show that the flow will exhibit a positive deviation from the slip-flow equation. According to Eqs. (2.44) and (2.45) the flow due to the slip term in the slip-flow equation is

$$Q_S = u_{o,\infty} A\ p = -\frac{a\varsigma}{2\eta}\frac{dp}{dx} A\ p . \tag{2.86}$$

Making use of $\zeta = 2\ c\ \lambda$ and $\eta = c\ m\ n\ v\ \lambda$, we get

$$Q_S = - \frac{a\ A\ p}{m\ n\ v} \left(\frac{dp}{dx}\right). \tag{2.87}$$

For a Maxwellian gas,

$$v^2 = \frac{8p}{\pi mn} \quad ;$$

thus Eq. (2.87) becomes

$$Q_S = - \frac{\pi}{8}\ v\ a\ A \frac{dp}{dx}\ . \tag{2.88}$$

The slip term using Eq. (2.84) is

$$Q_S' = u_{o,\infty} \left(1 - \frac{3}{16\gamma_a}\right) A\ p. \tag{2.89}$$

This can be rewritten

$$Q_S' = - \frac{\pi}{8}\ v\ a\ A \frac{dp}{dx} \left(1 - \frac{3}{16\gamma_a}\right)\ . \tag{2.90}$$

The flow due to diffusion is given by Hiby and Pahl to be

$$Q_D = - \frac{1}{3}\ v\ \lambda \left(1 - \frac{3}{16\gamma_a}\right) A \frac{dp}{dx}\ . \tag{2.91}$$

Adding Eqs. (2.90) and (2.91) and dividing by Eq. (2.88), we get

$$\frac{Q_S' + Q_D}{Q_S} = \left(1 + \frac{8}{3\pi\bar{\gamma}_a}\right)\left(1 - \frac{3}{16\gamma_a}\right) \tag{2.92}$$

or

$$\frac{Q_S' + Q_D}{Q_S} = 1 + \frac{1}{\gamma_a}\left(\frac{8}{3\pi} - \frac{3}{16}\right) - \frac{1}{2\pi\gamma_a 2}\ . \tag{2.92a}$$

Since γ_a is always much greater than 1 for slip flow, Eq. (2.92) is greater than 1. In addition, the velocity distribution across the duct is such that it will give a greater flow rate than the parabolic velocity distribution; thus the total flow rate must be greater than that calculated from the slip-flow equation.

Although only flow between parallel plates was considered, similar results should be obtained when the treatment is extended to channels with other cross sections.

Flow in the Molecular-Flow Region

Pollard and Present[25] considered self-diffusion in the molecular-flow region to be the sum of the flows occurring by two paths: a stream, Q_W resulting from molecules leaving the wall of the duct, and a stream Q_G resulting from molecules leaving points of gas collision. As a first approximation their solution can be extended to cover the case of flow. In their calculations of the stream Q_G, isotropic scattering of colliding molecules was assumed. Although this assumption is permissible in the self-diffusion calculation under uniform total pressure, gas collisions in the presence of a pressure gradient impart an average streaming velocity to the colliding molecules. In order to improve Pollard and Present's solution, we must take into account the additional flow due to streaming.

Let us consider a single collision between molecules. If these molecules have translational energy only, the total momentum of these molecules must be consderved after a collision. Furthermore, the sum of the components of momentum in any direction must be conserved. Thus the collision itself does not affect the total flow contribution of these molecules at the point of collision. Now let us consider the collisions that occur in an element of volume, dV. The probability that molecules coming from a given direction will collide in dV is independent of their direction of approach; therefore the average streaming velocity of a sufficiently large number of molecules colliding in dV is the same as the average velocity of the molecules passing through dV without colliding.

The total flow stream consists of molecules leaving the duct wall at a rate

$$N_W = (nv/4)\ 0 \quad \text{molecules per unit duct length}$$

and molecules leaving points of gas collision at a rate

$$N_G = (nv/\lambda)A \text{ molecules per unit length.}$$

Thus the fraction of the total flow due to streaming of the molecules under N_G is

$$\frac{N_G}{N_G + N_W} = \frac{(4A/\lambda\ 0)}{1 + 4A/\lambda\ 0} \quad . \tag{2.95}$$

This is the fraction of the total flow that Pollard and Present neglected by assuming isotropic scattering. Let the flow due to streaming be Q_T. Then

$$Q_T = \frac{4A/\lambda\ 0}{1 + 4A/\lambda\ 0} \quad Q \quad , \tag{2.96}$$

where Q is the total flow rate. But

$$Q = Q_D + Q_T, \tag{2.97}$$

where Q_D is the flow rate given by the self-diffusion equation; therefore

$$Q_T = (4A/\lambda\ 0)Q_D \tag{2.98}$$

and

$$Q = (1 + 4A/\lambda\ 0)\ Q_D. \tag{2.99}$$

For the cylindrical tube the limiting value of Q_T as a/λ approaches zero is

$$Q_T = \frac{4A^2 v}{\beta(0)} \frac{dp}{dx} (2a/\lambda). \tag{2.100}$$

This is greater than the corresponding quantities calculated by Hiby and Pahl[15] and by Weber.[29]

Hiby and Pahl derived the self-diffusion solution for infinite parallel plates by using the same assumptions as Pollard and Present:

$$Q_D = -8vaA \frac{dp}{dx} \left\{ \frac{\lambda}{6a} - \frac{\lambda^2}{32a^2} + \frac{\lambda^2}{8a^2} \left[\frac{e^{-\frac{2a}{\lambda}}}{4} \left(1 - \frac{10a}{3\lambda} - \frac{2a^2}{3\lambda^2} + \frac{4a^3}{3\lambda^3} \right) \right.\right.$$

$$\left.\left. + \left(\frac{2a^4}{3\lambda^4} - \frac{2a^2}{\lambda^2} \right) E \; i \; (-2a/\lambda) \right) \right] \right\} , \qquad (2.101)$$

where 2a is the separation between the plates. The additional flow due to streaming and the total flow are again given by Eqs. (2.98) and (2.99).

III. EXPERIMENTAL

Circular and Annular Sections

General Description

The over-all equipment is shown in Figs. 1 and 2. Gas is introduced into the system by feeding from a cylinder when a pure gas is used or by drawing from the room when air is used. Moisture in the air is removed with silica gel. The gas travels through a heat exchanger, which consists of a coil of 1/4-in. copper tubing immersed in a constant-temperature bath. This bath is maintained slightly above room temperature. The gas passes from the heat exchanger across two flowmeters which are also immersed in the same constant-temperature bath, and is then introduced into the vacuum system through two needle valves connected in series. The second needle valve is connected to a header which distributes the gas into the test section. Pressures are measured at two points along the test section by McLeod gauges. The discharge of the test section is connected to one leg of a 6-in. glass tee. The lower leg of the tee is connected to a high-speed baffle valve, to which the pumping unit is connected. To the third leg of the glass tee is attached a Pirani gauge, whose purpose is for monitoring only.

Flowmeters

It is necessary to thermostat the flowmeters so as to prevent changes in the pressure inside the flowmeter due to fluctuations of the room temperature during flow measurements.

The operation of a flowmeter can be illustrated with Fig. 3. When the flow of a new gas is to be measured the old gas is purged from the flowmeter through the purge stopcock by opening all the stopcocks on the flowmeter. (At other times the purge stopcock remains closed.) When the

pressure along the test section is being measured, gas is fed at constant pressure P_3 across the flowmeter. The pressure of the feed gas above the needle valves is obtained by adding the difference in heights between the mercury in the manometer leg and the body of the meter to the atmospheric pressure.

When the flow rate is measured, the pressure in the system is first increased above a predetermined value P_1 and the stopcock v_1 is closed. Henceforth the gas is drawn from the flowmeter. The time for the pressure to change from P_1 to P_2 (also predetermined) is recorded. From this the flow rate can be calculated.

Because the mechanism of flow across the needle valve changes with flow rate, the dependence of the flow rate on P varies between the first and second power. Equations of flow are derived in the Appendix for the cases wherein the flow rate is proportional to P_3 and P_3^2. It is shown there that when P_1/P_2 is less than 1.1, by measuring the rate of flow according to the relation $P_3 = (P_1 + P_2)/2$, we get almost identical answers with these equations. The flow rates in this work are calculated with the equation for the flow rate proportional to the first power of pressure,

$$Q = \frac{P_3}{t}\left[2A(P_1 - P_2) + (V_1 - AP_1)\ln\frac{P_1}{P_2}\right],$$

where A is the cross-section area of the manometer leg, and V_1 is the volume enclosed within the purge stopcock, the needle valve, the mercury seal, and v_1 when the pressure is P_1.

To cover the entire range of operation two meters are used, one with an approximate volume of 75 cc and the other of 1000 cc.

Header

A drawing of the header is shown in Fig. 4. A 65-mm-diameter fritted-

glass disc separates the header into two chambers. Gas enters the left chamber from the needle valves, diffuses through the glass disc, and distributes itself evenly into the test section from the right chamber.

Test Section

A 10.5-ft length of 3-in.(o.d.) standard 16 B.W.G. copper tube serves as the test section for measurement of flow through a circular section, and also serves as the outer tube of the annular sections. The upstream pressure tap is placed approximately 4 feet from the upstream end of the tube and the downstream pressure tap is approximately 1.5 feet from the downstream end. This leaves a 5.005-ft section across which the pressure drop is measured.

The circular section is converted to an annular section by centering a smaller copper tube within the 3-in. tube. The upstream end of the core is sealed by soldering on a copper disc, but the downstream end remains open. Measurements are made with cores of 1.5 and 2.5 in. in diameter.

Each end of the core is supported by three cap screws spaced at 120° intervals around the periphery of a 5-in. collar that is soldered to a flange plate. This is shown in Figs. 4 and 5. Additional support for the core is provided by legs soldered 120° apart to the core, 3.5 feet in from each supporting collar.

McLeod Gauges

The three McLeod gauges used to measure the pressure at the taps on the test section are shown in Fig. 6. The gauge in the center is used to measure pressures in the range from 0 to 100μ. The total volume of this gauge is approximately 1000 cc, and the tip and reference arm are made of 1.5-mm(i.d.) precision-bore capillaries. Between the pressure

range of 100μ and 300μ, the gauge on the left in Fig. 6 is used. It has a total volume of about 700 cc. and a tip of 3-mm. (i.d.) precision bore capillary. Pressures above 300μ are measured with the multirange McLeod gauge. Its total volume is 250 cc. and the inside diameter of the largest section of the tip, which is the only section used, is 10 mm.

Leads from the pressure taps are connected to a three-way vacuum stopcock so that either tap may be connected to the McLeod gauges. In this way the same gauge is used to measure both pressures whenever it is feasible. A cold trap is provided between the three-way stopcock and the McLeod gauges.

Pumping Unit

The pumping unit is best shown in Fig. 2. It consists of a 500-liters-per-second DPi oil diffusion pump, a 200-liters-per-second DPi oil diffusion booster pump, two cold traps, and a 5-cfm Kinney rotary pump. It is necessary to keep the pressure in the glass tee as low as possible so as to provide a large enough difference in pressure between the pressure taps to be accurately measured. In normal operation only the main diffusion pump and the rotary pump are used. Since the booster pump hardly increases the pumping capacity of the unit it is never used as such. The cold trap at the discharge of the main diffusion pump is used when the flow of CO_2 or Freon-12 is being measured.

Freon-12 and CO_2 can be pumped at flow rates higher than the capacity of the main diffusion pump by using the cold traps as pumps. To insure the lowest possible pressure in the cold traps they are backed by the booster pump and the rotary pump.

Two angle vacuum valves are located ahead of the cold traps to isolate the system when the cold traps are emptied or when the pumps are turned off.

Rectangular Section

Except for a header, a test section, and an adapter, the equipment for this part of the experimental work is essentially the same as that described above. Fig. 8 shows the apparatus with the rectangular section.

Header

A detailed drawing of the header is shown in Fig. 9. The header is constructed from 1/2-in. steel plates. To the face of one of the semi-circular plates, the needle valve through which the gas enters is soldered. The gas enters perpendicular to the direction of flow, passes through a fine-mesh screen which distributes the gas, and proceeds to the test section through a slit in the flange.

Test Section

The test section consists of two copper plates and a copper separator, forming a channel with a cross section of 1/8 in. by 9 in. and a length of 50 inches. The plates are identical except for the pressure taps in one of them. Two main pressure taps are centered on the plate with a distance of 24 inches between them. A third pressure tap is placed near the edge of the plate on a line perpendicular to the direction of flow from the upstream tap. This is used to check whether the pressure is constant across the channel. When no difference could be observed between the pressures at the upstream taps the one near the edge was plugged.

Both surfaces of each plate are ground to assure flatness. The grinding marks on the inner surface are then removed with fine emery cloth. The plates are sealed to the separator with O-rings made from 1/8-in. rubber stock. Grooves are cut on both sides of the separator to house the O-rings. The plates rest on the machined surfaces of the separator when they are drawn together.

Adapter

The adapter, like the header, is constructed from 1/2-in. steel plates. It is used to join the test section to the glass tee of the existing equipment. It is shown in Fig. 9.

Procedure

After leaks were removed from the system it was pumped down at no-flow condition until only a negligible difference was observed between the pressures at the two pressure taps. This could usually be accomplished with a week's pumping with the circular and annular sections. Because of the large gasket area exposed to the system with the rectangular section a pumping-down period of from 3 to 4 weeks was necessary to reduce the pressure difference to a negligible amount.

Whenever the flow of a new gas was measured, the flowmeters were purged with approximately 5 ft^3 of the new gas. Meanwhile some gas was also drawn into the system to clean up the manifold.

The flow rate of gases was controlled with the first needle valve only, while the second needle valve was left wide open. Steady state was reached very rapidly except when the flow rate was very small. In every case, when two successive pressure readings at the same pressure tap remained constant, the McLeod gauges were switched to measure the pressure at the other pressure tap, and at least two measurements were made there also. Finally the McLeod gauges were switched back to the first pressure tap to see whether the pressure had changed in the meantime. If the flow was found to be steady the flow rate was then measured. Except when very low flow rates were measured, for which cases the measurements were extremely time-consuming, at least two measurements were made for each flow setting.

IV. RESULTS AND DISCUSSION

Data were plotted in dimensionless form: Q/Q_A as a function of Knudsen number, X/λ, where

Q = flow rate

and

$$Q_A = \frac{4}{3} v \frac{A^2}{0} \frac{(p_1 - p_2)}{L} \tag{4.1}$$

The mean free path was calculated from the viscosity of the gas:

$$\lambda = \eta / cmnv.$$

We know that $mn = PM/RT$ and $v = (8RT/\pi M)^{1/2}$; therefore the equation for the mean free path can be rewritten

$$\lambda = (\pi RT/8M)^{1/2} \eta / cp.$$

In this work the results were based on Chapman's viscosity constant, $c = 0.499$. The pressure was taken as the average of the upstream and the downstream pressures, $(p_1 + p_2)/2$. Hence, when we let $c = 1/2$,

$$\lambda = (2\pi RT/M)^{1/2} \eta/(p_1 + p_2) .$$

Q_A is related to the molecular-flow equation by the expression

$$Q_M = K \left(\frac{2}{f} - 1\right) Q_A . \tag{4.2}$$

For the circular section K equals 1. For other sections the theoretically derived equations for molecular flow are usually quite complex; therefore it is convenient to use an equation of this form with values of K tabulated as a function of the geometry of the cross section.[4]

Figure 22 shows K as a function of b/a for the annular section. Figure 23 shows K as a function of b/a for the rectangular section. In each case as the channel gets narrower, K increases, and in the limit K becomes infinite.

When X/λ is small Q/Q_A is expected to approach the molecular-flow limit, $K(\frac{2}{f} - 1)$, and when X/λ approaches infinity Q/Q_A is expected to approach the slip-flow limit. The slip-flow limit in dimensionless form for annular and circular sections is

$$\left(\frac{Q}{Q_A}\right)_{X/\lambda \to \infty} = \frac{3\pi X}{64\lambda} + \left(\frac{2}{f} - 1\right) \frac{3\pi}{16} . \qquad (4.3)$$

Equation (2.49) can be used as the slip-flow limit for the rectangular section. When expressed in dimensionless form, Eq. (2.49) becomes

$$\left(\frac{Q}{Q_A}\right)_{X/\lambda \to \infty} = \frac{\pi a \phi}{16\pi} + \frac{3\pi}{16}\left(\frac{2}{f} - 1\right) . \qquad (4.4)$$

Molecular-Flow Region

The molecular-flow data were compared with molecular-flow equations for infinitely long channels. We know that the pressure gradient along a finite channel is not constant. It is greatest at the ends and goes through an inflection point in the center; most of the variation occurring at the ends. Calculations of the conductance of finite circular channels were made by Clausing[9] and Eberhardt.[13] According to their calculations the conductance of the tube in this work is 96% of the conductance of an infinite tube. When pressure taps were placed in the center portion of the tube the end effect was eliminated. Thus, the data should more closely approach the infinite-tube limit and we should be justified in comparing them with the infinite-tube equation.

Although the conductances of the other finite channels in this work are not known, we know that as the ratio L/X increases, the conductance approaches that for the infinite section also. Since the L/X ratios of the other sections were all greater than that for the tube, and since the pressure taps were also located in the center portions of these ducts, it should be

permissible to compare the results from these sections with equations for infinite sections also.

Figure 11 shows the data for flow in the circular section at lower values of a/λ. Within the experimental accuracy, the data appear to fall on three separate curves, with the hydrogen and helium data falling on the lowest curve, the air and carbon dioxide data on the middle curve, and the Freon-12 data on the highest curve. The three helium points and the hydrogen point at $a/\lambda = 0.01$ must be disregarded in drawing the lowest curve, since they were taken at such low flow rates and pressures that any leakage and outgassing -- as well as errors in the measurements of pressure -- would seriously affect their reliabilities. This statement applies to the accuracy of the data at low flow rates in the other sections as well. The curve drawn as long dashes is the best curve through Knudsen's and Gaede's data for flow of hydrogen, nitrogen, oxygen, and carbon dioxide in glass capillaries. This curve runs through the combined data for H_2, He, air, and CO_2 in this work over the entire range of measurement (see Fig. 15).

Several theoretical approximations of the variation of Q/Q_A with a/λ were also drawn in Fig. 11. The assumption that $f = 1$ was made in each of these approximations. The lowest curve is Pollard and Present's solution for self-diffusion in infinite tubes, and can be used as a first approximation of the flow. The second approximations take into account the streaming of the gas molecules due to intermolecular collisions. Curves representing the results from Hiby and Pahl, Weber, and this work are shown. In the region where they are applicable ($a/\lambda < 0.1$) the differences among them are small.

Although none of the data extended to low enough values of a/λ to allow the intercept to be determined, it appears that the hydrogen and helium data are approaching the second-approximation curves. This would indicate that f's for these gases are very close to 1. A fuller discussion of f is made later.

It is not possible to determine from the flow data which of the second approximations gives the closest flow prediction in the molecular-flow region, because not only must the data be very accurate, but also f must be known independently. For this reason the greatest advantage of the derivation in this work is its simplicity: once the self-diffusion solution in a channel is known, Eq. (2.99) can be used to predict the flow.

Figures 12 and 13 show the experimental data for flow at lower values of X/λ in the annular sections. Section AI has a ratio of diameters of 0.524, and section AII a ratio of diameters of 0.872. The corresponding values of K are 1.17 and 1.43. Figure 14 shows the data for flow in the rectangular section. For this section K is 2.08.

The following discussion applies to hydrogen and helium only, since they seem to be reflected from the wall with f = 1 in the circular section. In each channel Q/Q_A appears to be increasing toward the theoretical limit for molecular flow with decreasing X/λ, but the degree of approach at a given X/λ is poorer as the channel becomes narrower (as K increases). Self-diffusion solutions are not available for annular and rectangular sections; therefore no comparison of the data with theory can be made in the molecular-flow region. However, the solution for self-diffusion between infinite parallel plates was derived by Hiby and Pahl. From their solution the theoretical variation of Q/Q_A with X/λ was obtained with Eq. (2.99) and plotted in Figs. 14 and 19. This curve then represents the upper limit for

rectangular sections. The theoretical molecular-flow limit for the infinite parallel plates is infinity, but at $X/\lambda = 0.001$, Q/Q_A has only reached a value of 2.8.

Eberhardt showed that when molecular flow prevails, molecules traveling nearly parallel to the axis contribute only a small fraction of the total pressure drop in a tube, but contribute greatly to the molecular transport. When some intermolecular collisions occur, it is most likely for these molecules to have their paths interrupted, since they travel the furthest between wall collisions. For this reason the conductance in a tube initially decreases with increase in pressure.

This effect should be even more pronounced in narrower channels. Let us compare the molecular flows in a tube and between two parallel plates. In the tube those molecules leaving the wall nearly parallel to the axis will travel much farther before striking the wall again than those leaving parallel to the wall but at an angle with the axis because of the wall curvature. On the other hand those molecules leaving the flat surface parallel to the surface but at small angles with the direction of flow (axis) will contribute almost as much to the flow as the molecules traveling parallel to the axis. When intermolecular collisions occur in the parallel-plates channel, it is again most likely for these molecules that contribute greatly to the flow but only little to the momentum transport to have their paths interrupted. As these molecules contribute a greater fraction of the total flow in the parallel plates than in the tube, the initial decrease of the conductance with increasing pressure is more pronounced. The argument for the flat plates applies to the annular section also, because the walls appear flatter as b/a approaches 1. Thus,

it is not surprising that the theoretical molecular-flow limits were not observed experimentally in the annular and rectangular sections, at least for hydrogen and helium.

Similar results were obtained by Rasmussen. He found that the molecular-flow limits are not reached in his channels, all of which should have K's of around 2. One drawback in his data is that -- except for the annular section -- the theoretical molecular-flow limits for his particular channels were not known, and hence he compared his measurements with approximate limits that may or may not be correct.

The flow data for the annular sections fall on three separate curves just as they did for the circular section, with hydrogen and helium falling on the lowest curve, air and carbon dioxide falling on the middle curve, and Freon-12 falling in the highest curve. In the rectangular section the hydrogen data fall below the helium data at low X/λ's. The helium data fall in with the air and carbon dioxide data. Again, the Freon-12 data lie on the highest curve.

Transition-Flow Region

The minimum in the conductance of a channel lies in the transition-flow region. Only a shallow minimum was observed in the data for the circular section, but it becomes more pronounced in the annular and rectangular sections. The minimums of Q/Q_A for H_2, He, air, and CO_2 are approximately constant in all the channels and lie between 0.9 and 1.0. The minimums in the Freon-12 data are not very consistent. Rasmussen also observed that the minimums of Q/Q_A in his channels are all about 1.

Although Eq. (2.99) is not expected to hold too well -- if at all -- in the transition-flow region, it predicts minimums in this region for both the circular section and the infinite parallel plates. The predicted

minimum for the circular section is 0.95, while the minimum in the hydrogen and helium data is 0.92. The corresponding Knudsen numbers for the predicted and experimental minimums are not in very good agreement; but then, neither are the experimental minimums of Knudsen and Gaede, and of this work. Because of the shallowness of the curves, the exact position of the minimum is hard to determine accurately. The fraction of molecules diffusely reflected may have some effect on its position.

Hiby and Pahl's solution predicts a minimum of 0.92 in the tube at $a/\lambda \cong 0.1$, but then increases much more rapidly than the experimental data at higher Knudsen numbers. The good agreement between their minimum and the minimum in the H_2 and He data is probably coincidental, as their equation should hold only at small Knudsen numbers. In their derivation it was assumed that, at most, molecules suffer only one gas collision between wall collisions, a condition satisfied only at low Knudsen numbers.

The experimental minimum in the rectangular section is 0.97. Equation (2.99) predicts a minimum of 1.02 for the infinite parallel plates. This is in the right direction, for an increase in K shifts the curve upward in the molecular-flow region. This effect probably extends into the transition-flow region and thus causes the minimum value of Q/Q_A to increase. The Knudsen number at the minimums are in good agreement between the rectangular section and the infinite parallel plates.

As expected, Eq. (2.99) breaks down completely as the Knudsen number is further increased, going through a maximum and finally making an asymptotic approach to 1.

Slip-Flow Region

Most data in the slip-flow region in this work were taken with CO_2 and Freon-12, since only they could be pumped with the cold traps after the

main diffusion pump failed. Figure 15 shows the data for the copper tube in this work at larger Knudsen numbers and Cheng's[6] data for air and hydrogen in copper tubes. The curve through the data represents the best fit of Knudsen's and Gaede's data for flow through glass capillaries. This curve is also a good fit for the data by Cheng and from this work. The lower curve is that for the slip-flow equation. At $X/\lambda = 10$ the data fall much higher than the curve for the slip-flow equation. The agreement is better at large values of X/λ, but this is because the fraction of flow due to slip becomes smaller. The available slip-flow data in copper tubes scatter too much to establish whether or not the slip-flow limit is reached at large Knudsen numbers.

Figures 16 through 19 are log-log plots of all the experimental data in this work. The data for the annular and rectangular sections show more definitely that the respective slip-flow limits are reached at large Knudsen numbers. Meanwhile, as X/λ decreases, positive deviation from the slip-flow equation occurs in each channel.

The three separate curves for the different gases in the molecular flow region appear to converge to one curve in the slip-flow region. This is to be expected because f affects only the slip term of the slip-flow equation. Even so, if f is pressure-independent, a slight difference between the CO_2 and Freon-12 data should continue to be observed. In Tables IV through VII, column 7, are tabulated $(Q - Q_L)/Q_A$ in and near the slip-flow region. This function should approach $3\pi\left(\frac{2}{f} - 1\right)/16$ as X/λ increases, if the slip-flow equation is valid. An inspection of the data shows no systematically greater flow of Freon-12 over CO_2 in this region, except in the tube. Although this may be due to the inaccuracy of the measurements, the pressure in the system may conceivably affect f for Freon-12.

A comparison of the data for the circular and annular sections in the slip-flow region at a given X/λ shows that the deviation from the slip-flow equation is largest for the circular section and smallest for section AII. Since at a given X/λ, X is largest for the tube, the corresponding pressure in the tube must be lowest. Consequently, if the curvature of the wall has any effect on the deviation, it will be greatest in the tube. Thus, even though the slip-flow limit was not reached by the experimental data for the circular section, we can reasonably speculate that it is reached at higher pressures.

Fraction of Molecules Diffusely Reflected

Where the equations for molecular flow are known, it should be possible to evaluate f from experimental data in the molecular-flow region by extrapolating them to $X/\lambda = 0$. However, the experimental data are not accurate enough nor do they extend to low enough X/λ's to be used in this manner. Pollard and Present showed that the slope of Q/Q_A at $X/\lambda = 0$ is infinite, which adds greatly to the inaccuracy of any extrapolation.

Alternately, it is possible to evaluate f from slip-flow data. Normally, one would expect to use the data in the range, $10 < X/\lambda < 100$, because the flow is not expected to follow the slip-flow equation at lower X/λ's and the slip-flow contribution to the flow at larger X/λ's is too small to be accurately measured. It was shown in Chapter III that the noncontinuum nature of the gas causes a positive deviation from the slip-flow equation. This deviation could be appreciable in the range of usable data. Consequently, f's calculated from these data tend to be low.

Although the data do not extend to low enough values of X/λ to be used for determining f directly, the data in the circular section indicate that f for hydrogen and helium is very close to 1. If the flow data for

these gases were extrapolated toward zero, parallel to Knudsen's and Gaede's data in Fig. 11, the intercept would be very close to 1. In addition, these data appear to approach the second approximation curves of Hiby and Pahl, of Weber, and of this work, which are based on f = 1. Accordingly, the assumption that f = 1 was made for hydrogen, and f's for the other gases were evaluated relative to hydrogen. This was done by comparing the flows at chosen values of X/λ. From the ratio of the flow rates of a gas and hydrogen, f of the gas can be calculated from the equation

$$\frac{(Q/Q_A)_{gas}}{(Q/Q_A)_{H_2}} = \frac{2}{f} - 1,$$

as long as we remain in the molecular-flow region. Actually, it was not always possible to use only data in the molecular-flow region to evaluate f. However, f's calculated from data in the lower range of the transition-flow region are not noticeably different from those calculated from data in the molecular-flow region. The results of these calculations are set forth in Table III. The following average values of f were obtained by giving equal weight to each channel:

Gas	H_2	He	Air	CO_2	Freon-12
f	1.00	0.99	0.97	0.97	0.90 .

These calculations indicate that there is a dependence of f on the molecular weight of the gas, although the differences among the f's of the first four gases are small. In previous works most measurements were carried out with different surfaces, but the gases used in these measurements were usually H_2, air, CO_2, O_2, or N_2. The data in this work show that f's for these gases are all very close to 1 for copper surfaces. If this applies

to other surfaces as well, then those investigators would not observe any large effect of a gas on f. Adzumi made flow measurements of H_2, C_2H_2, and C_3H_6 in a glass capillary and found no large deviation of f from 1 in the molecular-flow limit.

Empirical Correlation of Experimental Data

The semiempirical equation used by Knudsen to correlate his experimental flow data through glass capillaries is

$$Q = Q_L \left[1 + \frac{64\lambda}{3\pi a} \left(\frac{1 + C_1 a/\lambda}{1 + C_2 a/\lambda} \right) \right] . \qquad (4.4)$$

This equation can be rearranged:

$$Q = Q_A \left[\frac{3\pi a}{64\lambda} + \frac{1 + C_1 a/\lambda}{1 + C_2 a/\lambda} \right] . \qquad (4.5)$$

Knudsen's equation reduces to Q_A, the molecular-flow equation for tubes, when $a/\lambda = 0$. When $a/\lambda \longrightarrow \infty$, the equation becomes

$$Q = Q_L \left[1 + \frac{64 C_1 \lambda}{3\pi C_2 a} \right] . \qquad (4.6)$$

If $C_1/C_2 = 3\pi/64$, Eq. (4.6) becomes the slip-flow equation. Knudsen found that his data are best fitted by $C_1/C_2 = 0.81$ and $C_2 = 5.00$. However, with these constants Knudsen's equation will not reduce to the slip-flow equation.

The correlating equation used in this work is similar to Knudsen's. The equation for annular and circular sections has the form

$$Q = Q_A \left[\frac{3\pi X}{64\lambda} + K \left(\frac{1 + C_1 (X/\lambda)^{C_2}}{1 + (16KC_1/3\pi)(X/\lambda)^{C_2}} \right) \right] . \qquad (4.7)$$

This equation reduces to the theoretical molecular-flow limit when $X/\lambda = 0$ and to the approximate slip-flow limit, Eq. (2.17), when $X/\lambda \longrightarrow \infty$. The intermediate range is fitted by adjusting C_1 and C_2. On a log-log plot of $(Q/Q_A - 3\pi X/64\lambda)$ as a function of X/λ, C_2 determines the shape of the curve

while C_1 determines its position along the abscissa. For the circular and annular sections the same value of 0.4 for C_2 was found to give good fits for the shapes of the curves. The values found for C_1 are: 0.276 for the circular section, 1.00 for section AI, and 1.32 for section AII. The empirical equations are shown as dotted lines in Figs. 16, 17, and 18.

The curve representing Rasmussen's data for a glass annular section (b/a = 0.9984) is shown in Fig. 20. Equation (4.7) can be fitted to his data with the constants $C_1 = 1.54$ and $C_2 = 0.4$.

Figure 21 shows a plot of C_1 as a function of b/a. A straight line can be drawn through these points. The equation of this line is

$$C_1 = 0.275 + 1.27b/a \ . \tag{4.8}$$

When we substituted Eq. (4.8) into Eq. (4.7), we get a general empirical equation for flow in annular and circular sections,

$$Q = Q_A \left[\frac{3\pi X}{64\lambda} + K \left(\frac{1 + (0.276 + 1.27b/a)(X/\lambda)^{0.4}}{1 + (16K/3\pi)(0.275 + 1.27b/a)(X/\lambda)^{0.4}} \right) \right] \tag{4.9}$$

In the absence of flow data Eq. (4.9) can be used to calculate flow in annular section in the range $0 < b/a < 0.9984$. The behavior of this equation as b/a approaches closer to 1 is not known, but it is unlikely that such a channel is normally used.

The correlating equation for the rectangular section has the same form as Eq. (4.7):

$$Q = Q_L + KQ_A \left(\frac{1 + C_1(2a/\lambda)^{C_2}}{1 + (16K/3\pi)C_1(2a/\lambda)^{C_2}} \right), \tag{4.10}$$

where the laminar flow limit Q_L is given by Eq. (2.43). For the rectangular section in this work the values of $C_1 = 1.23$ and $C_2 = 0.3$ are found to give a good fit of the data.

When the fraction of the molecules diffusely reflected is not 1, the last term of these empirical equations should be multiplied by the factor $(\frac{2}{f} - 1)$.

Acknowledgments

The author is indebted to Professors L. A. Bromley and D. N. Hanson for their parts in directing this work, to his friends and associates who have helped to make the task a pleasant one, to Mrs. Robert Waite for the numerous time she has assisted him, and to the U.S. Atomic Energy Commission for its sponsorship of this project.

Table III

Fraction of molecules diffusely reflected in this work

		f				
Channel	X/λ	H_2	He	Air	CO_2	Freon-12
Circular	0.02	1.0	1.0	0.96	0.96	-
	0.2	1.0	1.0	0.96	0.96	0.88
Section AI	0.05	1.0	1.0	0.96	0.96	0.84
	0.5	1.0	1.0	0.96	0.96	0.87
Section AII	0.03	1.0	1.0	0.98	0.98	0.88
	0.5	1.0	1.0	0.98	0.98	0.97
Rectangular	0.01	1.0	0.96	0.96	0.96	0.92
	0.1	1.0	0.98	0.98	0.98	0.94
Average*		1.0	0.99	0.97	0.97	0.90

*The averages were obtained by giving equal weight to each channel.

Table IV

Flow measurements in the circular section

$a = X = 3.64$ cm

Exp. No.	p_1 μ	p_2 μ	$\frac{Q}{u\text{-}l}$ sec	T °C	$\frac{Q}{Q_A}$	$\frac{X}{\lambda}$	$\frac{Q-Q_L}{Q_A}$
Hydrogen							
1	0.041	0.020	1.92	19.2	0.903	0.0138	
2	0.071	0.033	3.84	20.8	0.975	0.0232	
3	0.161	0.062	9.35	20.5	0.915	0.0500	
4	0.269	0.118	14.5	17.8	0.934	0.0875	
5	0.737	0.276	43.9	20.7	0.920	0.227	
6	1.95	0.742	117	20.7	0.933	0.602	
7	7.60	2.95	532	20.2	1.106	2.37	
Helium							
8	0.040	0.010	1.85	21.1	0.870	0.0071	
9	0.042	0.016	1.75	20.2	0.918	0.0084	
10	0.058	0.017	2.51	20.6	0.822	0.0106	
11	0.139	0.048	6.38	21.1	0.951	0.0265	
12	0.386	0.130	17.6	21.6	0.936	0.0730	
13	1.59	0.527	70.7	21.8	0.906	0.299	
14	3.64	1.25	166	21.7	0.947	0.690	
15	12.9	5.09	673	21.0	1.174	2.54	
Air							
16	0.066	0.024	1.15	21.7	0.994	0.0365	
17	0.110	0.037	1.98	21.7	0.996	0.0606	
18	0.471	0.158	8.39	20.8	0.982	0.258	

Table IV (Page 2)

Exp. No.	p_1 μ	p_2 μ	$\frac{Q}{u\text{-}l}$ sec	T °C	$\frac{Q}{Q_A}$	$\frac{X}{\lambda}$	$\frac{Q-Q_L}{Q_A}$
19	1.76	0.577	33.5	21.6	1.04	0.962	
20	4.88	1.87	108	21.4	1.31	2.77	
21	14.7	6.53	481	20.9	2.14	8.70	0.86
Carbon Dioxide							
22	0.037	0.014	0.519	19.9	1.01	0.0323	
23	0.105	0.035	1.49	19.3	0.959	0.0886	
24	0.368	0.122	5.46	20.2	1.00	0.312	
25	2.76	0.980	48.9	20.1	1.14	2.37	
26	12.1	5.58	352	19.1	2.44	11.3	0.77
27	21.9	10.8	925	19.9	3.79	20.8	0.72
Freon-12							
28	0.084	0.034	0.784	20.0	1.19	0.147	
29	0.134	0.050	1.28	19.3	1.15	0.231	
30	0.154	0.058	1.51	21.1	1.18	0.262	
31	0.185	0.065	1.88	20.5	1.17	0.312	
32	0.302	0.107	2.97	18.4	1.14	0.515	
33	1.19	0.455	13.1	19.1	1.32	2.02	
34	4.32	1.90	70.4	19.0	2.17	7.81	1.12
35	6.01	2.84	113	19.8	2.78	10.1	1.29
36	9.88	4.93	245	19.1	3.73	18.6	0.99
37	35.4	29.2	1050	20.2	12.7	80.6	0.8
38	41.5	35.2	1280	19.5	15.2	96.1	1.0

Table V

Flow measurements in annular section AI

a = 3.64 cm, b = 1.905 cm, X = 1.165 cm

Exp. No.	p_1 μ	p_2 μ	$\frac{Q}{u\text{-}l}$ sec	T °C	$\frac{Q}{Q_A}$	$\frac{X}{\lambda}$	$\frac{Q-Q_L}{Q_A}$
Hydrogen							
39	0.162	0.064	3.66	22.9	0.929	0.0143	
40	0.297	0.101	7.23	21.6	0.936	0.0251	
41	0.796	0.284	19.1	22.1	0.941	0.0675	
42	3.28	0.957	82.6	21.6	0.897	0.266	
43	5.45	1.62	140	21.3	0.926	0.442	
44	13.7	4.11	369	21.8	0.968	1.12	
45	13.9	4.16	374	21.6	0.976	1.13	
46	18.9	5.81	518	21.9	1.01	1.54	
47	21.5	6.92	601	22.0	1.05	1.76	
Helium							
48	0.077	0.027	1.42	23.2	1.00	0.0042	
49	0.271	0.087	5.18	22.7	0.985	0.0143	
50	0.660	0.205	13.0	23.2	0.985	0.0345	
51	2.78	0.802	52.5	22.8	0.927	0.144	
52	8.58	2.45	164	23.1	0.928	0.441	
53	10.2	2.89	193	20.2	0.914	0.529	
54	31.5	9.80	651	23.1	1.04	1.65	
55	32.6	10.1	669	19.8	1.04	1.73	
56	35.4	11.3	729	20.1	1.05	1.89	

Table V (Page 2)

Exp. No.	p_1 μ	p_2 μ	$\frac{Q}{u\text{-}l}$ sec	T °C	$\frac{Q}{Q_A}$	$\frac{X}{\lambda}$	$\frac{Q-Q_L}{Q_A}$
Air							
57	0.142	0.041	1.13	22.1	1.06	0.0214	
58	0.300	0.081	2.29	21.8	0.984	0.0442	
59	0.594	0.171	4.50	21.9	1.00	0.0893	
60	1.23	0.328	9.31	22.1	0.970	0.182	
61	1.94	0.523	14.7	22.7	0.972	0.286	
62	6.09	1.91	45	22.0	1.01	0.926	
63	13.8	4.32	113	21.5	1.12	2.11	
64	17.0	5.52	148	21.9	1.21	2.63	
65	36.5	13.2	406	21.4	1.64	5.78	0.79
66	43.5	16.4	522	21.1	1.80	7.00	0.77
Carbon Dioxide							
67	0.088	0.028	0.562	23.1	1.08	0.0208	
68	0.163	0.039	1.05	23.1	0.973	0.0456	
69	0.289	0.082	1.94	22.6	1.08	0.0663	
70	0.330	0.086	2.15	22.7	1.02	0.0744	
71	0.962	0.250	6.13	23.3	.996	0.216	
72	3.81	1.05	24.5	23.1	1.02	0.865	
73	9.40	2.79	66.1	23.3	1.16	2.17	
74	16.2	5.54	126	22.6	1.37	3.88	
75	25.4	9.21	229	22.6	1.63	6.18	0.72
76	29.3	10.9	285	22.1	1.78	7.19	0.72
77	63.9	27.3	975	22.0	3.10	16.4	0.68
78	96.7	74.0	993	21.8	5.10	30.7	0.57
79	169.7	132.6	2690	21.7	8.39	54.2	0.40

Table V (Page 3)

Exp. No.	p_1 μ	p_2 μ	$\frac{Q}{u\text{-}l}$ sec	T °C	$\frac{Q}{Q_A}$	$\frac{X}{\lambda}$	$\frac{Q-Q_L}{Q_A}$
Freon-12							
80	0.146	0.049	0.644	20.9	1.28	0.0695	
81	0.159	0.046	0.884	24.2	1.51	0.0715	
82	0.296	0.102	1.22	22.5	1.21	0.140	
83	0.387	0.107	1.53	20.9	1.05	0.176	
84	1.01	0.282	4.22	21.3	1.12	0.541	
85	1.70	0.485	7.00	23.0	1.12	0.770	
86	6.44	1.96	30.7	24.1	1.31	2.93	
87	7.40	2.30	36.7	22.4	1.39	3.42	
88	8.90	2.94	43.1	19.2	1.39	4.24	
89	9.57	3.32	48.8	22.4	1.49	4.53	
90	12.2	4.43	67.3	21.6	1.66	5.88	
91	15.0	5.70	89.8	21.5	1.85	7.35	0.77
92	32.8	14.2	304	20.9	3.14	16.7	0.68
93	63.7	41.3	705	22.5	6.07	37.0	0.62
94	67.1	43.6	751	21.1	6.16	39.2	0.38
95	72.3	47.2	873	21.1	6.69	42.4	0.46
96	73.0	48.1	924	21.6	7.12	42.9	0.79
97	103.3	68.5	1670	22.3	9.24	60.6	0.31
98	139.6	94.3	2970	23.0	12.5	82.0	0.4
99	153.6	104.8	3460	21.0	13.8	92.5	0.2

Table VI

Flow measurements in annular section AII

a = 3.64 cm, b = 3.174 cm, X = 0.3128 cm

Exp. No.	p_1 μ	p_2 μ	$\frac{Q}{u\text{-}l}$ sec	T °C	$\frac{Q}{Q_A}$	$\frac{X}{\lambda}$	$\frac{Q-Q_L}{Q_A}$
Hydrogen							
100	0.126	0.031	0.372	20.6	1.10	0.0027	
101	0.304	0.077	0.889	20.7	1.13	0.0064	
102	0.428	0.106	1.19	19.6	1.04	0.0092	
103	0.779	0.192	2.23	20.3	1.07	0.0167	
104	0.991	0.240	3.01	18.5	1.13	0.0213	
105	1.94	0.452	5.63	19.4	1.07	0.0413	
106	4.06	0.952	11.0	20.2	1.00	0.0862	
107	5.40	1.23	14.6	20.1	.987	0.114	
108	24.6	5.64	62.9	19.4	.934	0.520	
109	37.0	8.69	93.9	19.7	.937	0.787	
110	100	26.1	278	19.6	1.06	2.18	
111	157	44.9	482	20.0	1.20	3.47	
112	209	65.0	698	18.3	1.37	4.74	0.67
Helium							
113	0.071	0.017	0.134	18.9	1.00	0.00096	
114	0.281	0.070	0.651	19.3	1.23	0.0038	
115	0.387	0.096	0.872	18.8	1.19	0.0053	
116	0.750	0.182	1.73	19.0	1.21	0.0102	
117	0.912	0.216	1.96	19.0	1.12	0.0123	
118	3.40	0.800	7.14	19.2	1.09	0.0459	

Table VI (Page 2)

Exp. No.	p_1 μ	p_2 μ	$\frac{Q}{u\text{-}l}$ sec	T °C	$\frac{Q}{Q_A}$	$\frac{X}{\lambda}$	$\frac{Q-Q_L}{Q_A}$
119	12.5	2.80	24.5	19.1	0.952	0.158	
120	35.2	7.77	65.4	17.5	1.01	0.505	
121	120	29.6	231	18.5	0.945	1.53	0.72
122	288	84.7	652	18.9	1.27	4.06	0.67
Air							
123	0.237	0.058	0.199	22.3	1.19	0.0093	
124	0.838	0.200	0.654	20.2	1.09	0.0327	
125	0.958	0.226	0.760	20.7	1.11	0.0382	
126	2.32	0.526	1.74	20.1	1.03	0.0893	
127	5.4	1.19	3.92	20.1	0.992	0.208	
128	18.1	4.08	12.8	21.4	0.974	0.695	
129	54.3	13.9	40.6	20.5	1.07	2.14	
130	74.9	20.4	60.3	20.4	1.18	3.00	0.74
131	192	66.9	217	19.9	1.86	8.20	0.65
132	318	124	485	19.5	2.67	14.0	0.61
Carbon Dioxide							
133	0.539	0.120	0.324	18.5	1.05	0.0318	
134	1.30	0.290	0.824	18.7	1.07	0.0779	
135	6.30	1.37	3.56	18.4	0.951	0.376	
136	51.9	14.4	33.7	18.2	1.18	3.26	0.70
137	152	55.1	152	18.8	2.01	9.90	0.55
138	238	95.1	320	19.3	2.94	16.2	0.55

Table VI (Page 2)

Exp. No.	p_1 μ	p_2 μ	$\frac{Q}{u\text{-}l/sec}$	T °C	$\frac{Q}{Q_A}$	$\frac{X}{\lambda}$	$\frac{Q-Q_L}{Q_A}$
Freon-12							
139	0.247	0.060	0.117	17.9	1.37	0.0298	
140	0.493	0.110	0.216	20.5	1.23	0.0578	
141	1.48	0.312	0.514	20.4	0.966	0.173	
142	1.25	0.252	0.516	19.7	1.14	0.144	
143	3.13	0.627	1.15	20.6	1.00	0.358	
144	4.05	0.851	1.42	20.4	0.970	0.474	
145	11.1	2.56	3.71	20.4	0.951	1.32	0.76
146	29.7	8.89	50.6	20.5	2.19	10.6	0.63
147	180	78.9	194	18.1	4.19	25.1	0.59

Table VII

Flow measurements in the rectangular section

$2b = 0.324$, $2b = 22.86$, $X = 0.324$

Exp. No.	p_1 μ	p_2 μ	$\frac{Q}{u\text{-}l}$ sec	T °C	$\frac{Q}{Q_A}$	$\frac{X}{\lambda}$	$\frac{Q-Q_L}{Q_A}$
Hydrogen							
148	0.0500	0.026	0.128	22.6	1.18	0.00315	
149	0.076	0.027	0.281	23.0	1.24	0.0018	
150	0.081	0.031	0.287	22.5	1.23	0.0020	
151	0.106	0.048	0.347	22.1	1.30	0.0027	
152	0.126	0.052	0.470	23.6	1.36	0.0031	
153	0.198	0.078	0.734	23.2	1.31	0.0049	
154	0.213	0.086	0.737	21.9	1.27	0.0053	
155	0.238	0.098	0.854	22.5	1.31	0.0059	
156	0.514	0.181	1.70	22.4	1.10	0.0123	
157	0.493	0.184	1.71	22.4	1.19	0.0120	
158	0.518	0.205	2.00	23.3	1.37	0.0128	
159	1.44	0.613	4.70	22.9	1.18	0.0359	
160	13.0	4.41	39.5	23.8	1.00	0.304	
161	32.2	11.2	92.9	23.5	0.963	0.760	
162	148	59.1	447	23.6	1.09	3.62	0.74
163	424.6	309.3	965	23.2	1.83	12.9	0.47
164	1491	1240	5620	23.1	4.87	40.8	0.90

Table VII (Page 2)

Exp. No.	p_1 μ	p_2 μ	$\frac{Q}{u\text{-}l}$ sec	T °C	$\frac{Q}{Q_A}$	$\frac{X}{\lambda}$	$\frac{Q-Q_L}{Q_A}$
Helium							
165	0.066	0.030	0.139	21.3	1.19	0.00011	
166	0.055	0.019	0.153	22.4	1.27	0.00082	
167	0.101	0.045	0.267	22.6	1.47	0.00162	
168	0.155	0.059	0.407	20.7	1.28	0.00239	
169	0.175	0.073	0.492	22.2	1.48	0.00287	
170	0.198	0.073	0.522	20.7	1.26	0.00303	
171	0.225	0.082	0.650	21.7	1.37	0.00342	
172	0.300	0.107	0.830	21.3	1.31	0.00455	
173	0.300	0.113	0.881	22.4	1.42	0.00459	
174	0.384	0.150	1.06	22.4	1.39	0.00594	
175	0.360	0.144	1.06	22.2	1.49	0.00563	
176	0.413	0.163	1.14	20.7	1.41	0.00644	
177	0.682	0.243	1.92	21.1	1.32	0.0103	
178	0.676	0.249	1.94	22.7	1.38	0.0104	
179	1.326	0.487	3.68	22.7	1.35	0.0202	
180	3.41	1.22	8.66	22.6	1.20	0.0518	
181	13.6	4.73	30.2	22.4	1.04	0.204	
182	104	37.3	215	20.7	0.993	1.58	
183	261	105	579	21.1	1.15	4.10	0.75
184	960	681	2090	21.7	2.31	18.3	0.55
Air							
185	0.102	0.041	0.099	23.5	1.33	0.0046	
186	0.268	0.097	0.271	23.7	1.31	0.0117	
187	0.567	0.205	0.584	22.8	1.33	0.0248	

Table VII (Page 3)

Exp. No.	p_1 μ	p_2 μ	$\frac{Q}{u\text{-}l}$ sec	T °C	$\frac{Q}{Q_A}$	$\frac{X}{\lambda}$	$\frac{Q-Q_L}{Q_A}$
188	1.61	0.557	1.51	22.7	1.18	0.0697	
189	5.66	1.89	4.92	23.8	1.08	0.242	
190	34.2	12.2	26.1	21.5	1.00	1.53	
191	189	86.2	192	22.0	1.55	8.87	0.69
192	1493	1105	3920	22.2	8.40	84.0	0.28
Carbon Dioxide							
193	0.062	0.027	0.027	22.2	0.81	0.0044	
194	0.232	0.085	0.184	21.0	1.27	0.0158	
195	0.385	0.136	0.301	21.7	1.23	0.0259	
196	0.395	0.140	0.309	21.6	1.24	0.0267	
197	0.630	0.218	0.502	21.0	1.25	0.0423	
198	1.06	0.354	0.799	21.3	1.16	0.0704	
199	4.97	1.66	3.23	20.5	1.00	0.332	
200	6.61	2.19	4.19	19.1	0.976	0.446	
201	12.4	4.26	7.70	21.5	0.972	0.828	
202	31.5	11.6	19.3	19.9	0.994	2.16	
203	82.4	44.4	49.1	22.3	1.32	6.29	0.71
204	77.7	32.7	54.8	21.5	1.24	5.50	0.70
205	212	106	230	20.1	2.23	15.9	0.68
206	278	145	342	20.3	2.64	21.2	0.58
207	310	176	384	22.5	2.91	24.1	0.56
208	544	315	1019	25.0	4.52	42.0	0.43
209	567	331	1066	24.0	4.59	44.1	0.20
210	1192	712	4320	25.2	9.24	93.0	0.16

Table VII (Page 4)

Exp. No.	p_1 μ	p_2 μ	$\frac{Q}{u\text{-}l}$ sec	T °C	$\frac{Q}{Q_A}$	$\frac{X}{\lambda}$	$\frac{Q-Q_L}{Q_A}$
Freon-12							
211	0.143	0.056	0.072	21.9	1.40	0.0194	
212	0.439	0.150	0.212	22.6	1.24	0.0575	
213	0.506	0.172	0.250	20.4	1.27	0.0670	
214	1.15	0.376	0.522	21.1	1.14	0.150	
215	2.17	0.718	0.996	25.0	1.16	0.278	
216	3.96	1.29	1.57	21.4	0.994	0.515	
217	19.4	6.99	7.38	24.1	1.00	2.55	0.75
218	118.4	60.1	77.4	24.7	2.24	17.3	0.56
219	241	133	260	25.1	4.05	36.0	0.55
220	612	366	1385	25.0	9.51	94.3	0.33
221	1857	1162	11870	25.0	28.8	291	0.5

Table VIII

Fraction of molecules diffusely reflected

Surface	Gases	f	Source
Brass	air, CO_2	1.00	24
Mercury	air	1.00	24
Old shellac	air, CO_2	1.00	24
Oil	air	0.895	24
Oil	CO_2	0.92	24
Oil	H_2	0.925	24
Oil	He	0.874	24
Fresh shellac	air	0.79	24
Ag_2O	H_2, He	0.99-1.00	5
Ag_2O	air	0.97-0.98	5
Ag_2O	O_2	0.96-0.99	5
Steel	air, N_2	1.00	17
Polished Al	air, N_2	1.00	17
Unpolished glass	air, N_2	0.97	17
Glass *	air	0.89	24
Copper #	H_2	1.00	this work
Copper #	He	0.99	this work
Copper #	air, CO_2	0.97	this work
Copper #	Freon-12	0.90	this work

*Calculated by Millikan from Knudsen's and Warburg's slip-flow data.

#The f for H_2 was assumed to be 1 and the f's for the other gases were calculated relative to H_2.

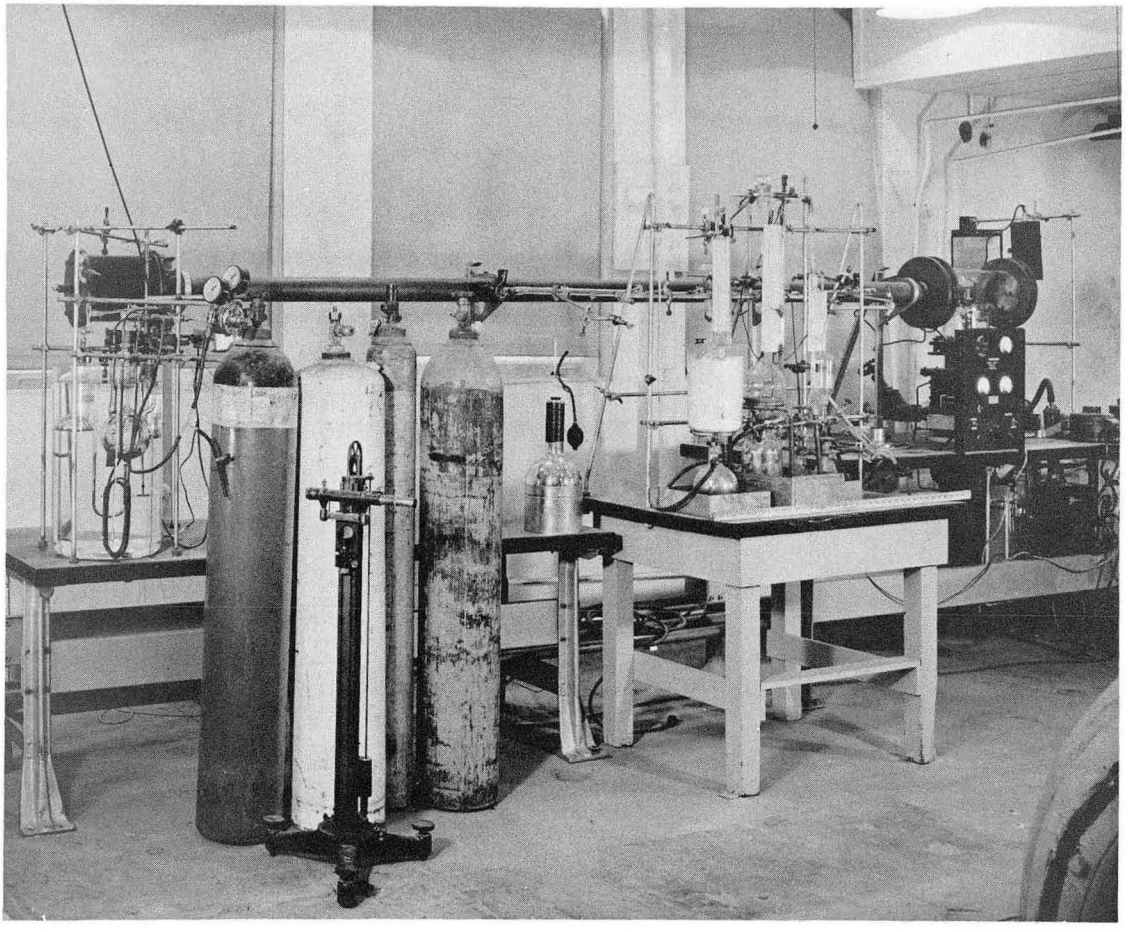

ZN-1488

Fig. 1. Experimental apparatus for measuring flow in circular and annular sections.

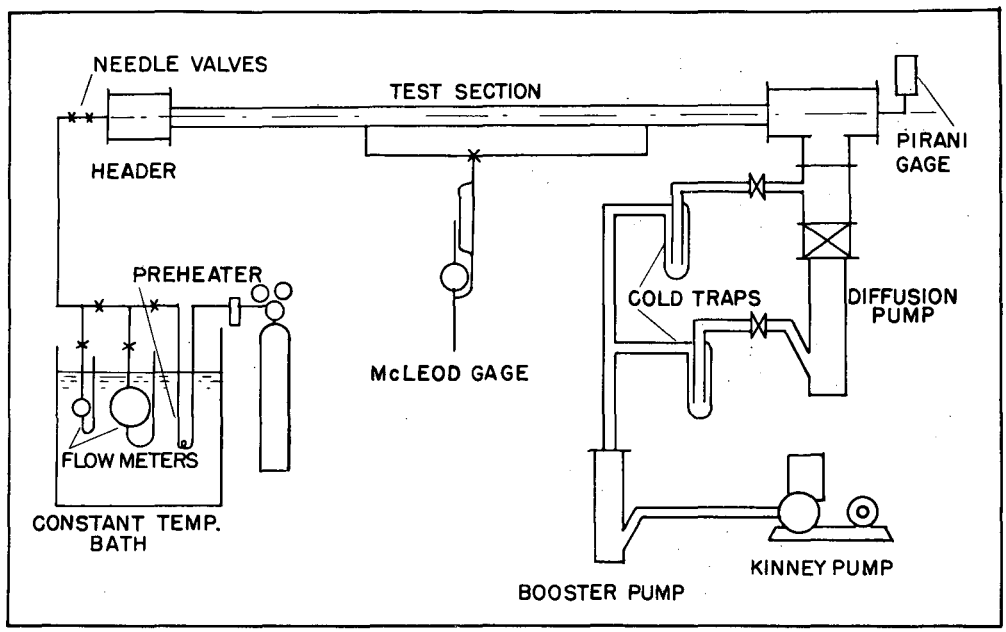

Fig. 2. Diagrammatic sketch of the apparatus for measuring flow in circular and annular sections.

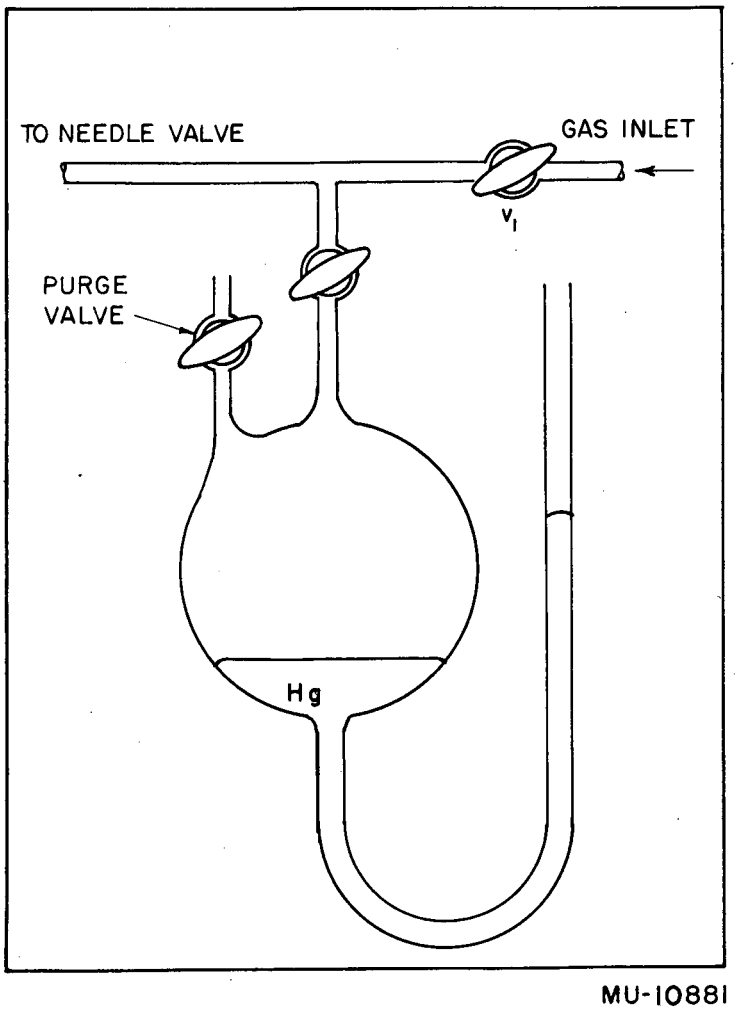

Fig. 3. Flow meter.

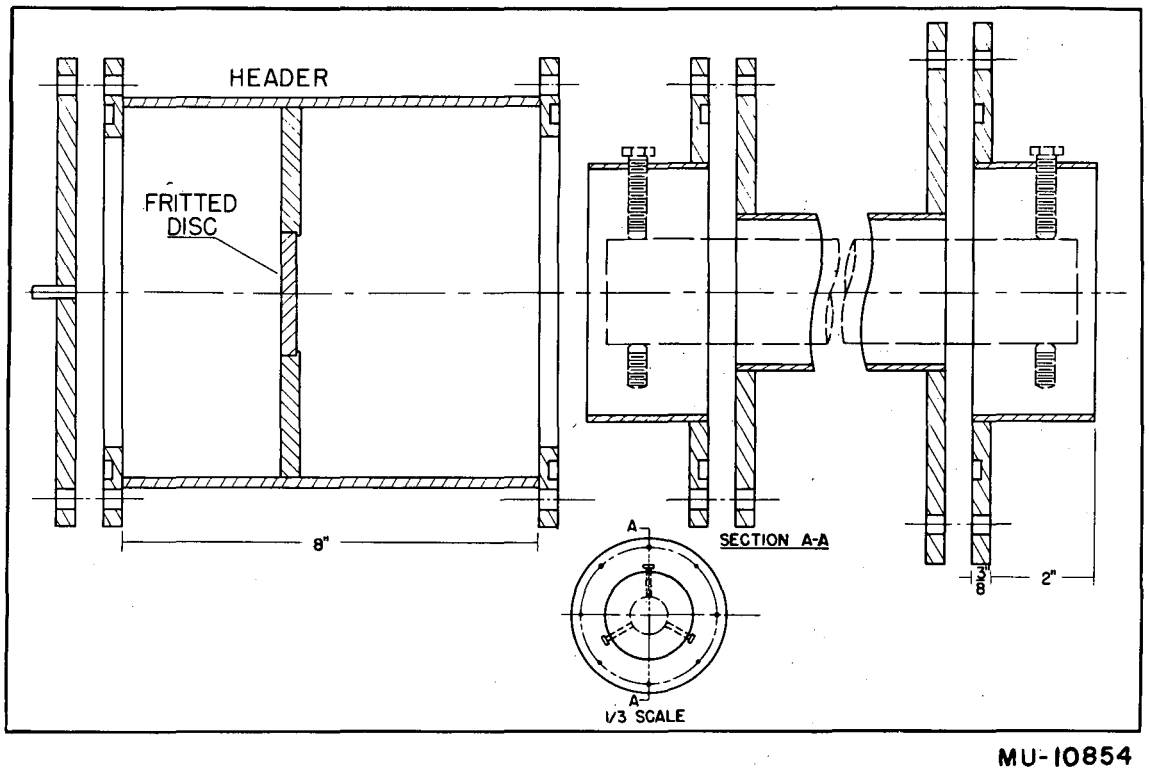

Fig. 4. Detailed drawing of the header and core supports - circular and annular sections.

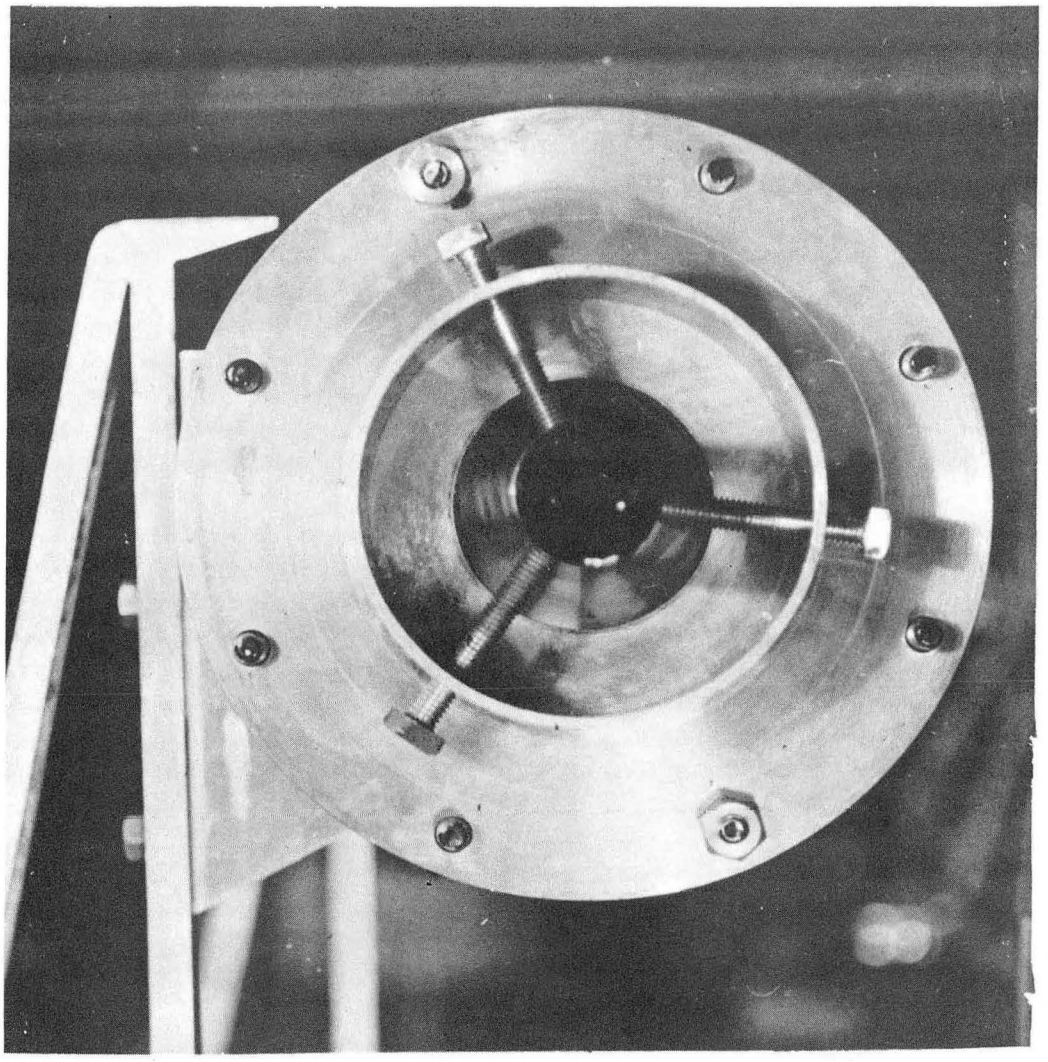

ZN-1491

Fig. 5. Upstream core support.

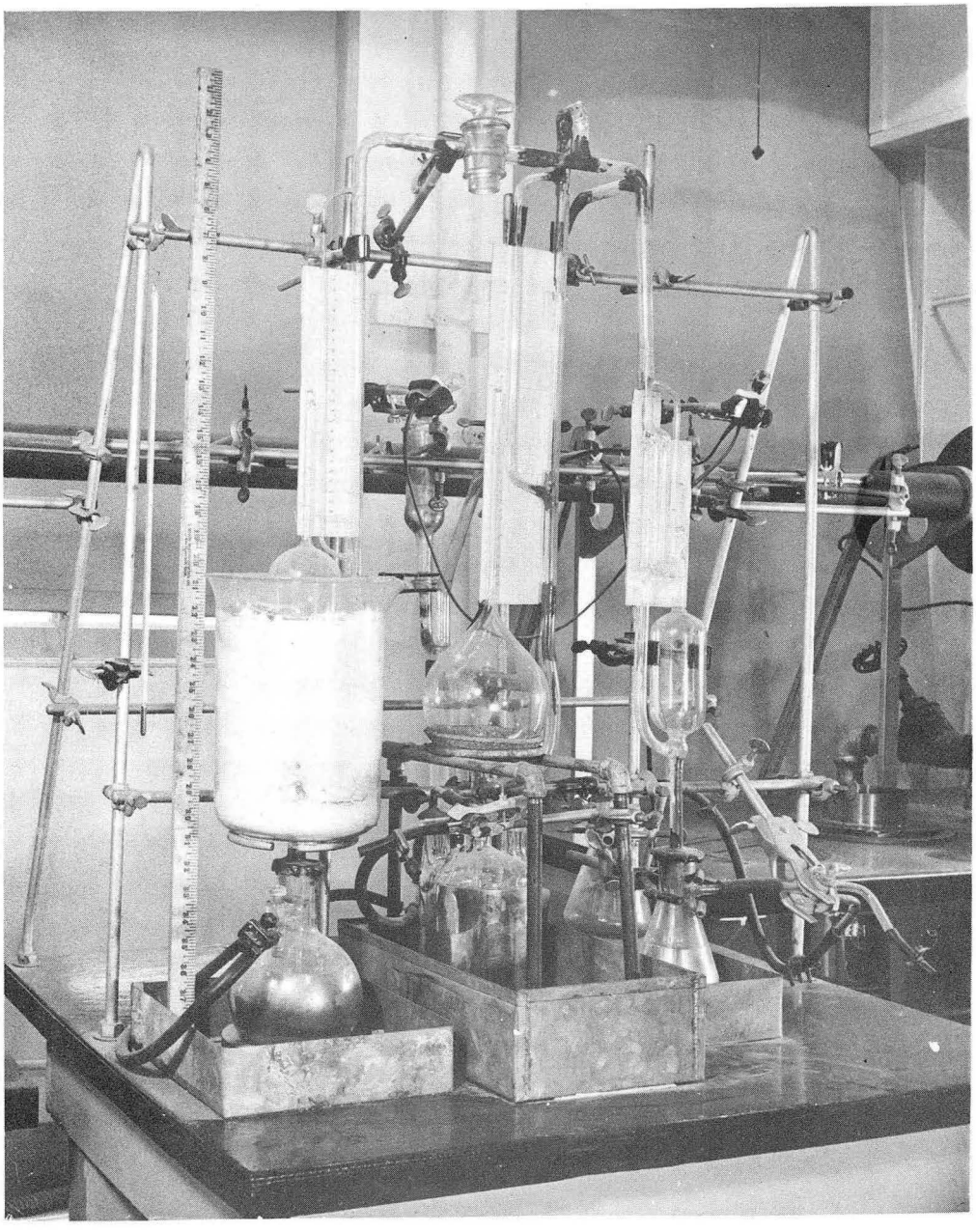

ZN-1490

Fig. 6. McLeod gauges.

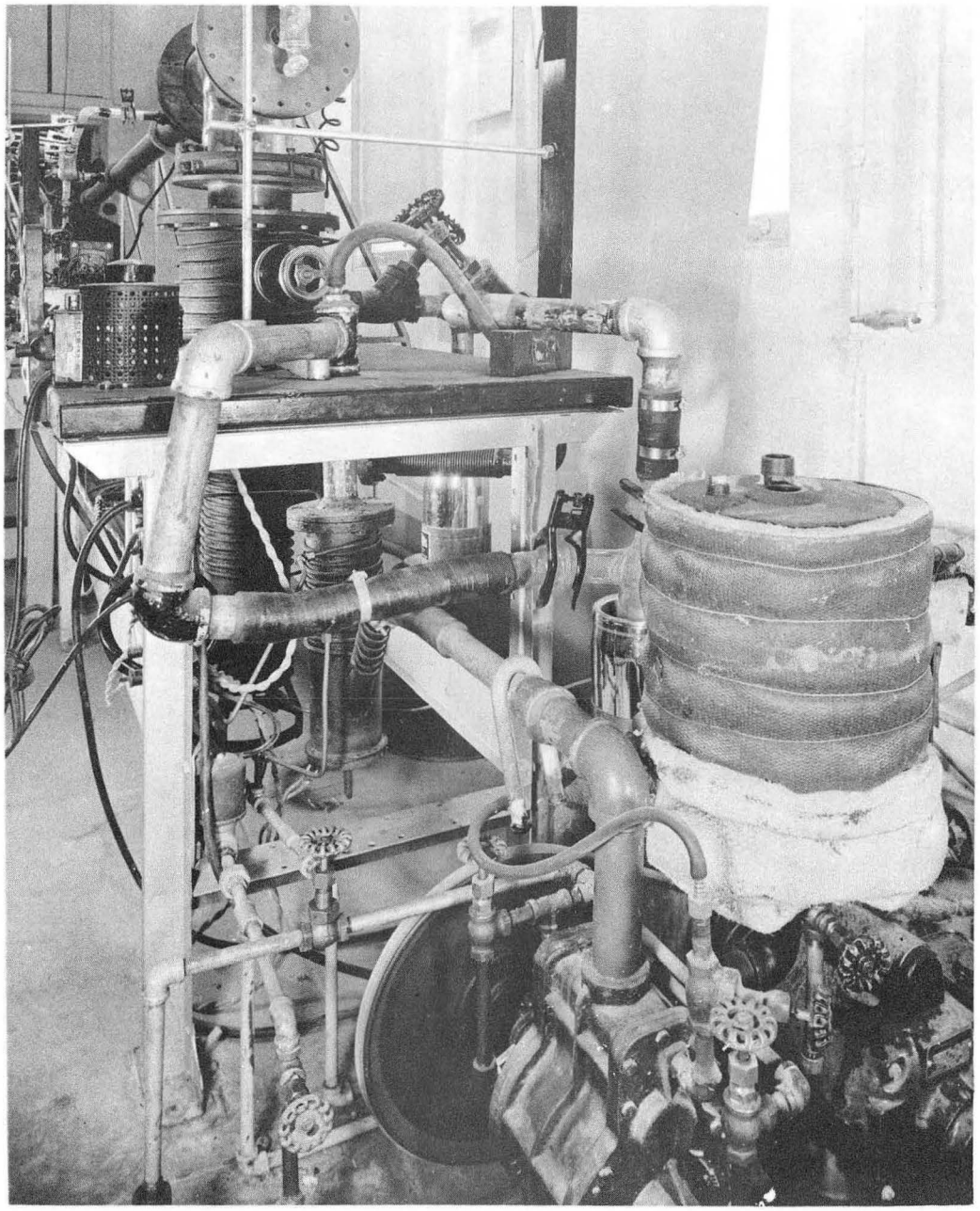

ZN-1489

Fig. 7. Pumping unit.

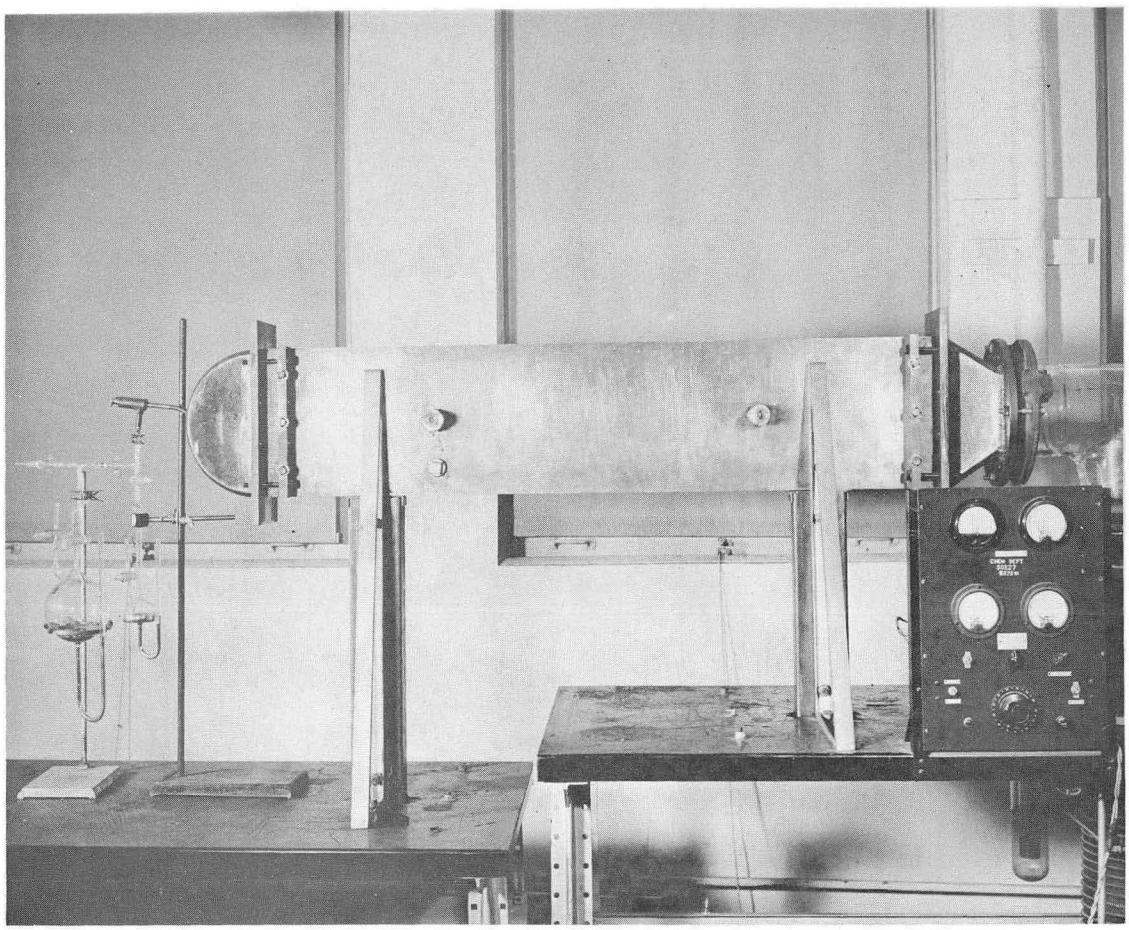

ZN-1487

Fig. 8. Header, rectangular test section, and adapter. Flow meters are shown on the left, removed from the thermostat.

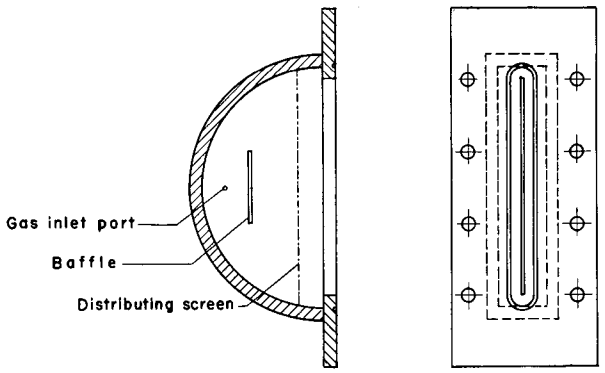

HEADER

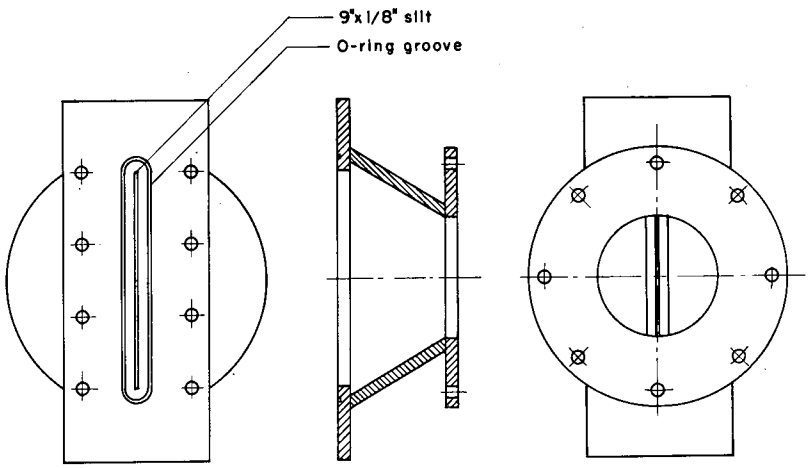

ADAPTER - RECTANGULAR SECTION

MU-1088'.

Fig. 9. Header and adapter - rectangular section.

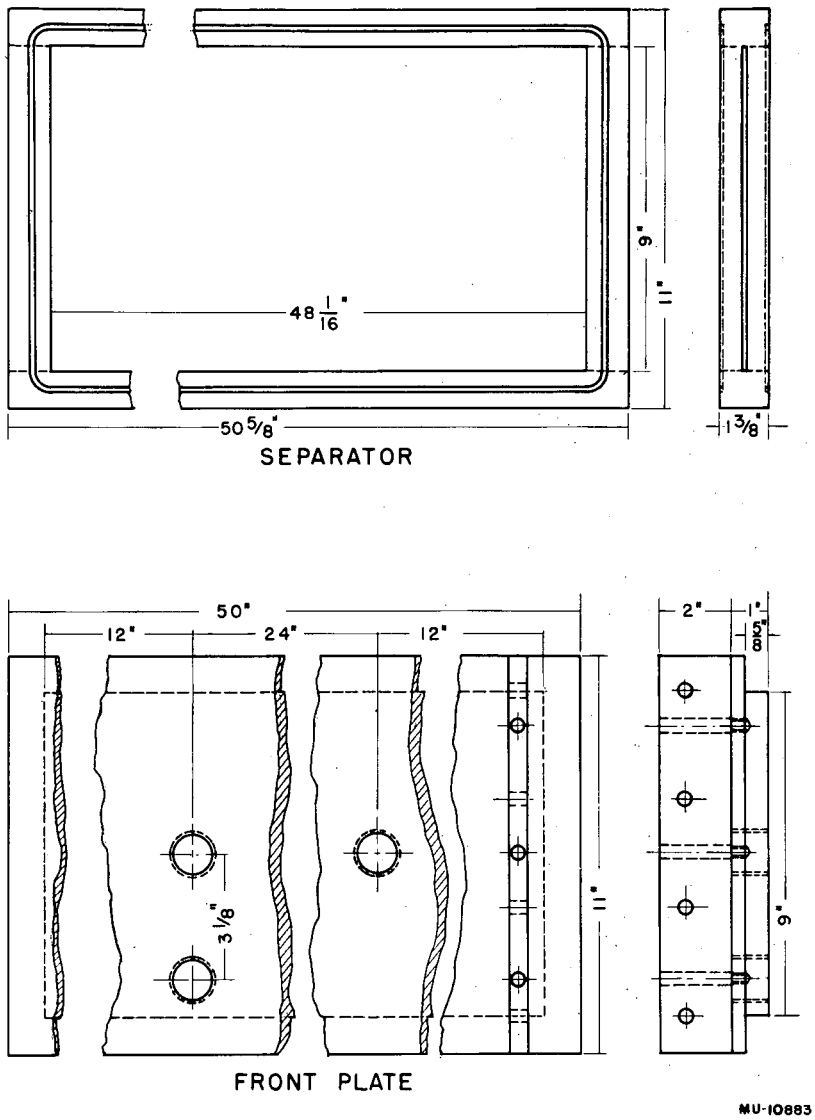

Fig. 10. Detailed drawing of the rectangular test section.

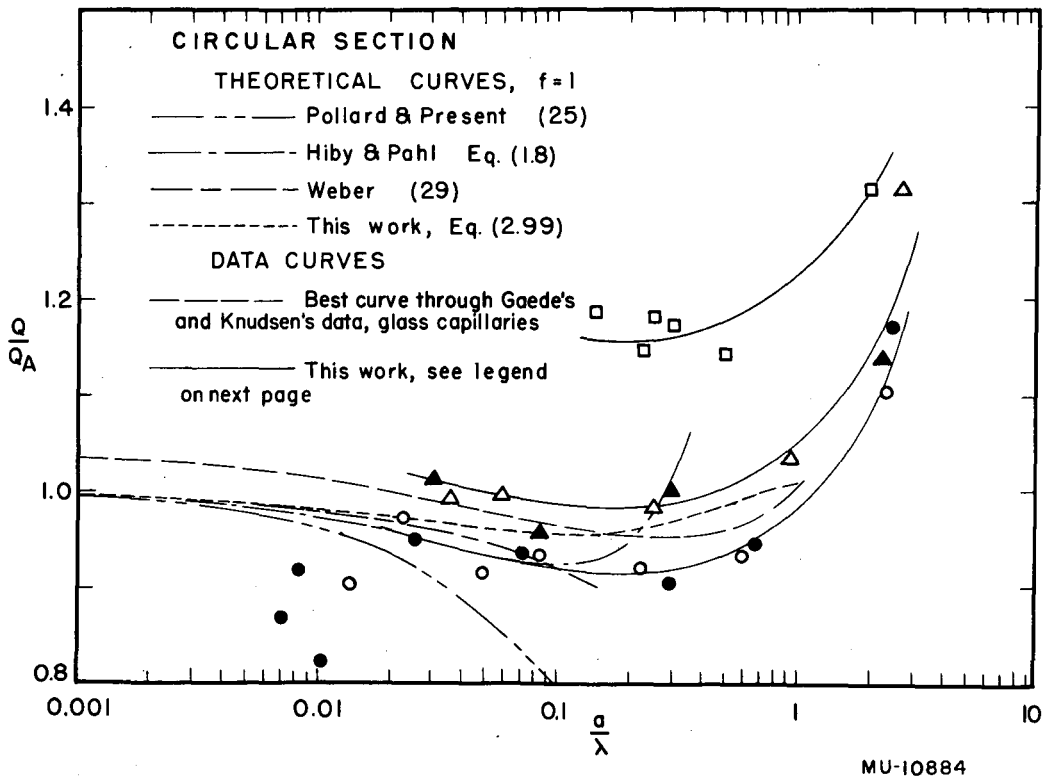

Fig. 11. Flow data and theoretical approximations in the molecular and transition flow regions in the circular sections.

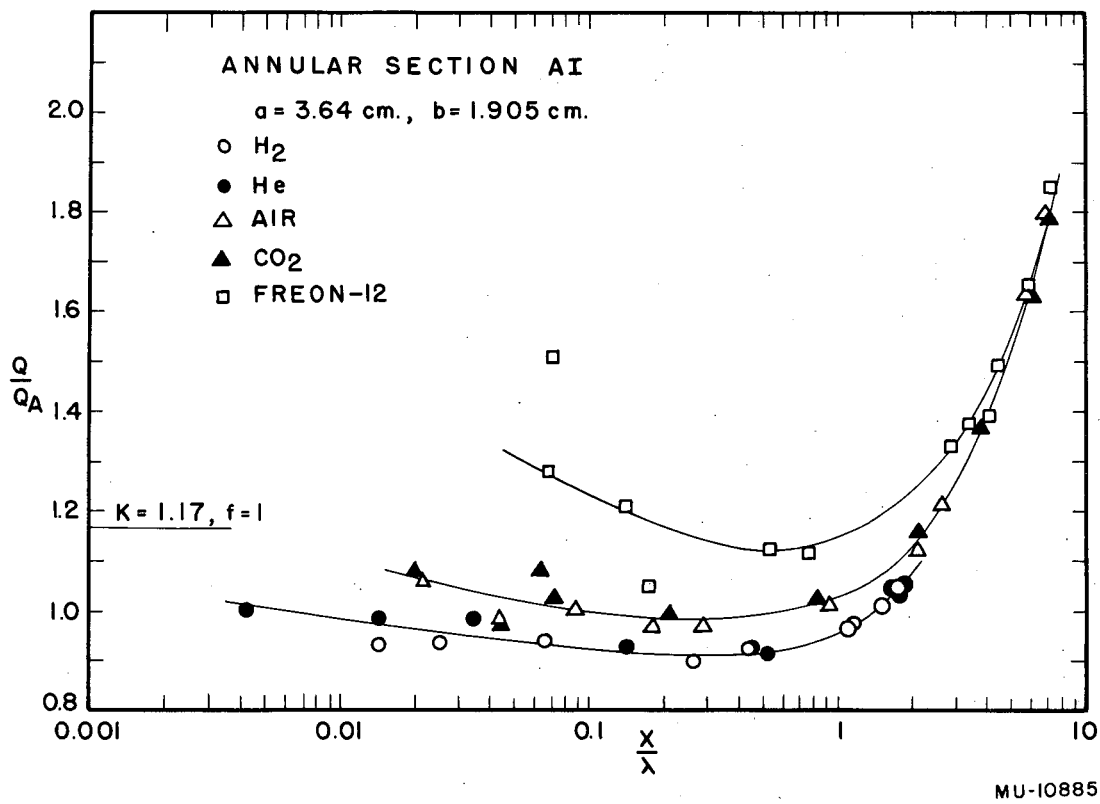

Fig. 12. Flow data in the molecular and transition flow regions in annular Section AI.

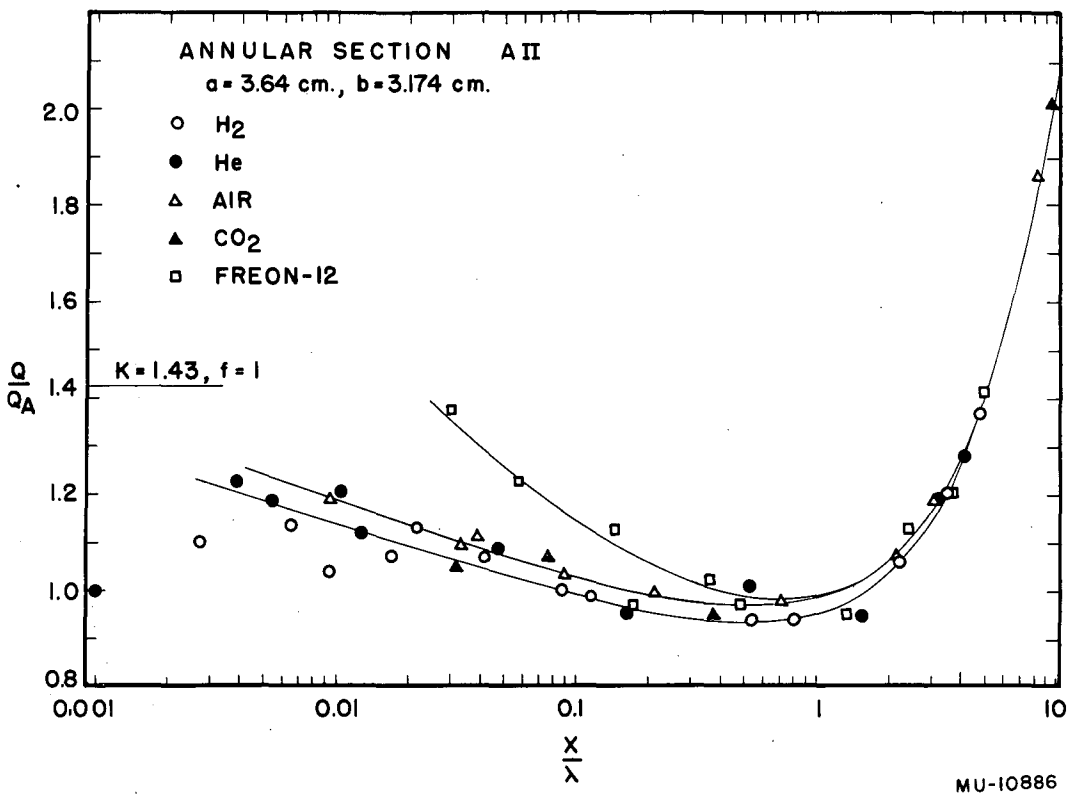

Fig. 13. Flow data in the molecular and transition flow regions in annular Section AII.

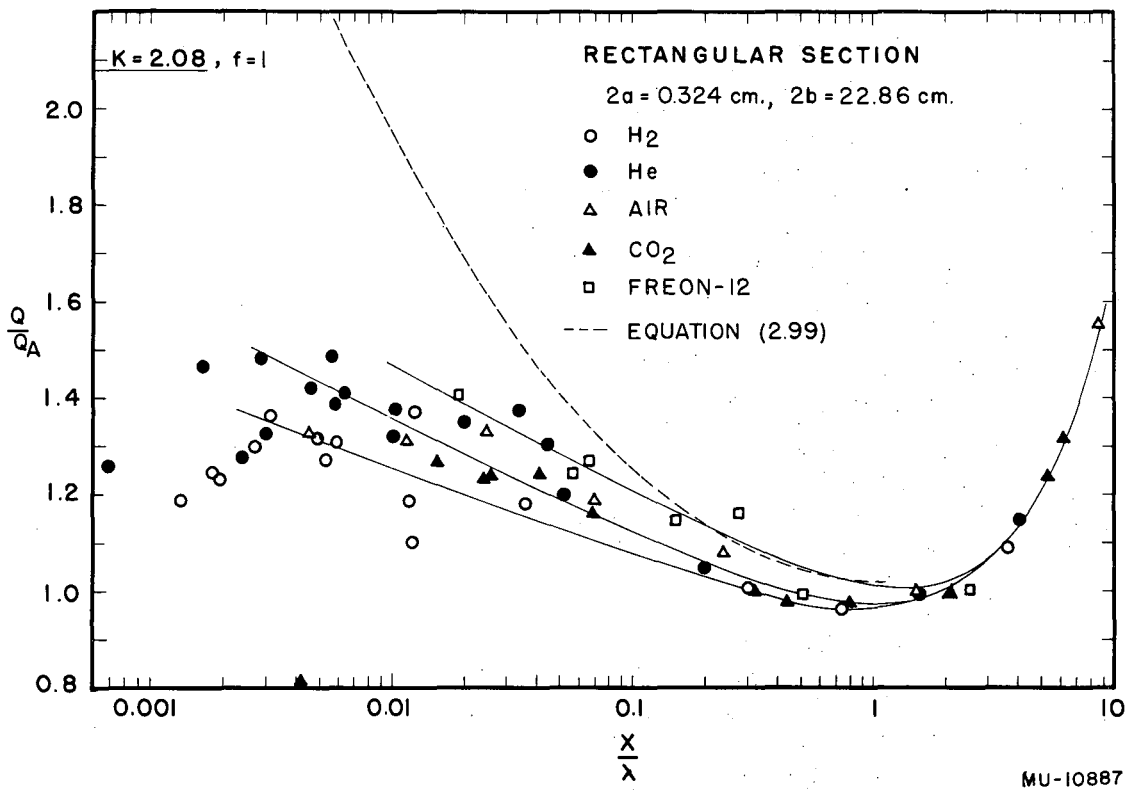

Fig. 14. Flow data in the molecular and transition flow regions in the rectangular section.

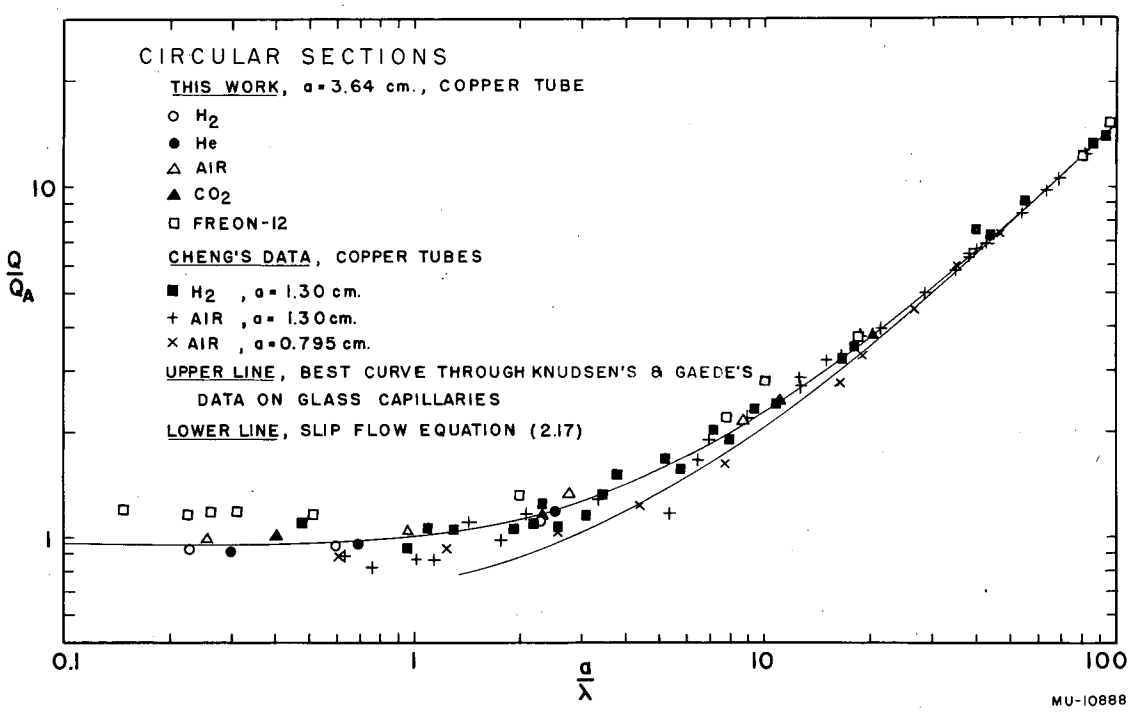

Fig. 15. Flow data of Cheng, Knudsen, Gaede, and this work in the slip flow region in circular sections.

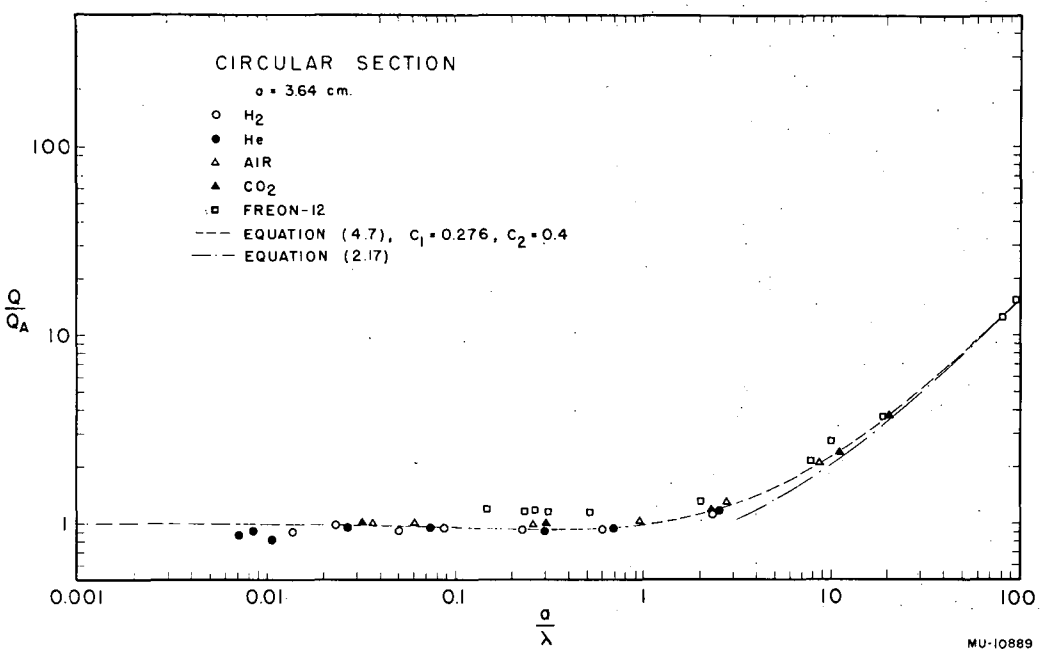

Fig. 16. Flow data in the circular section.

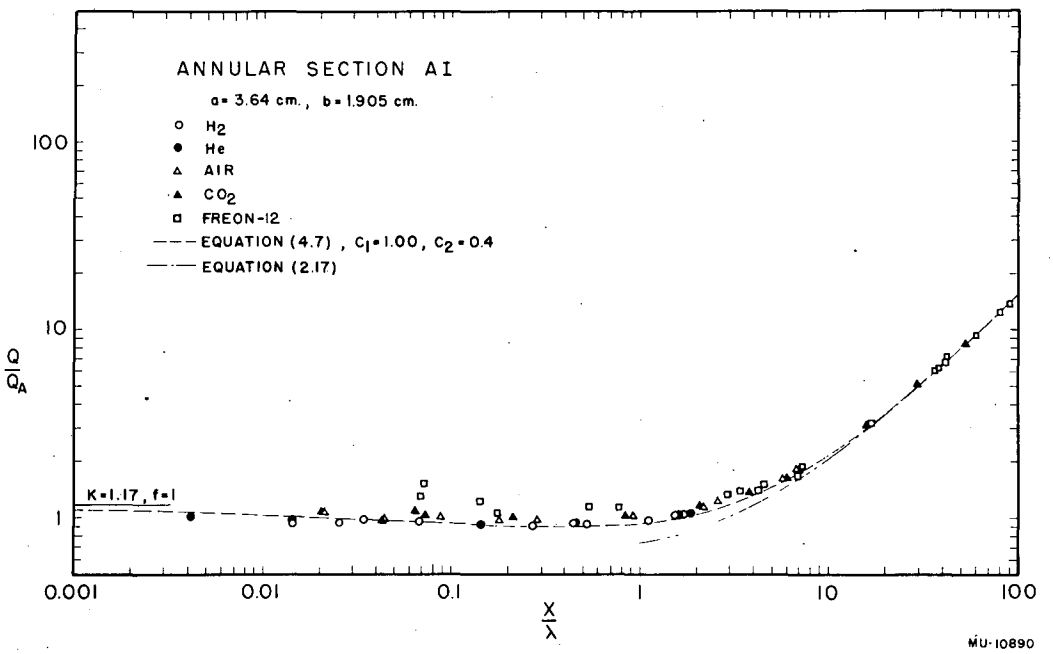

Fig. 17. Flow data in annular Section AI.

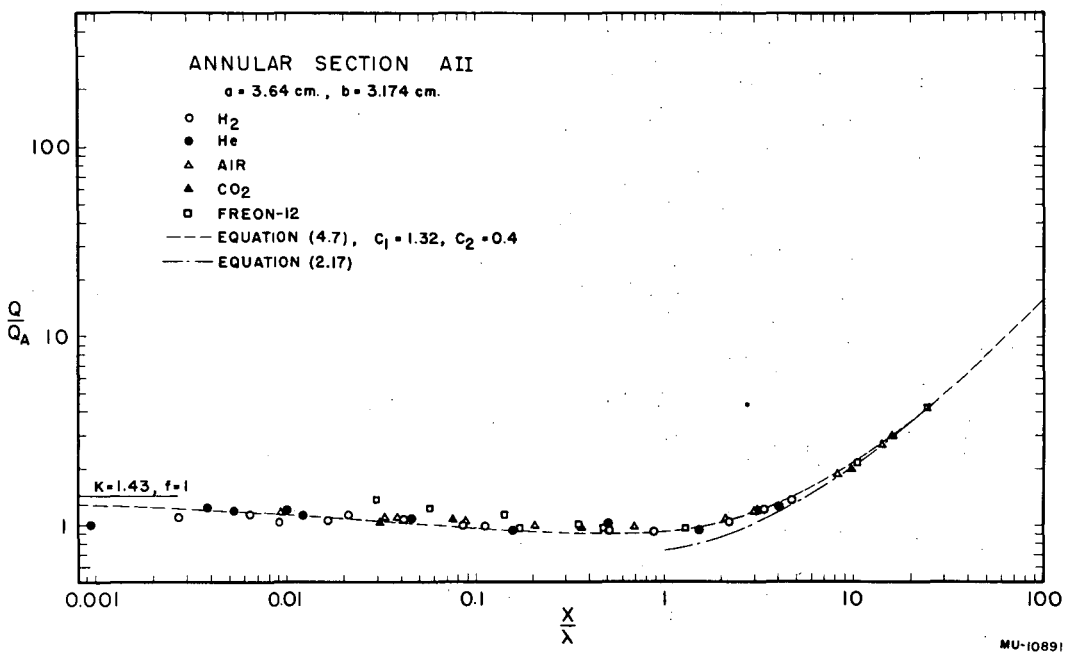

Fig. 18. Flow data in annular Section AII.

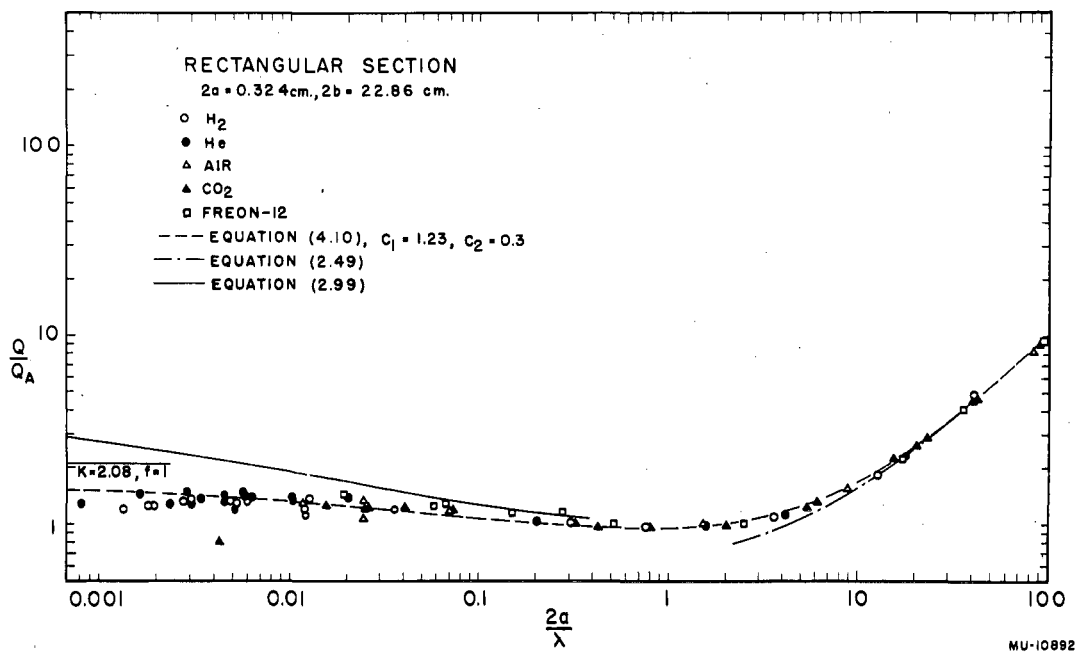

Fig. 19. Flow data in the rectangular section.

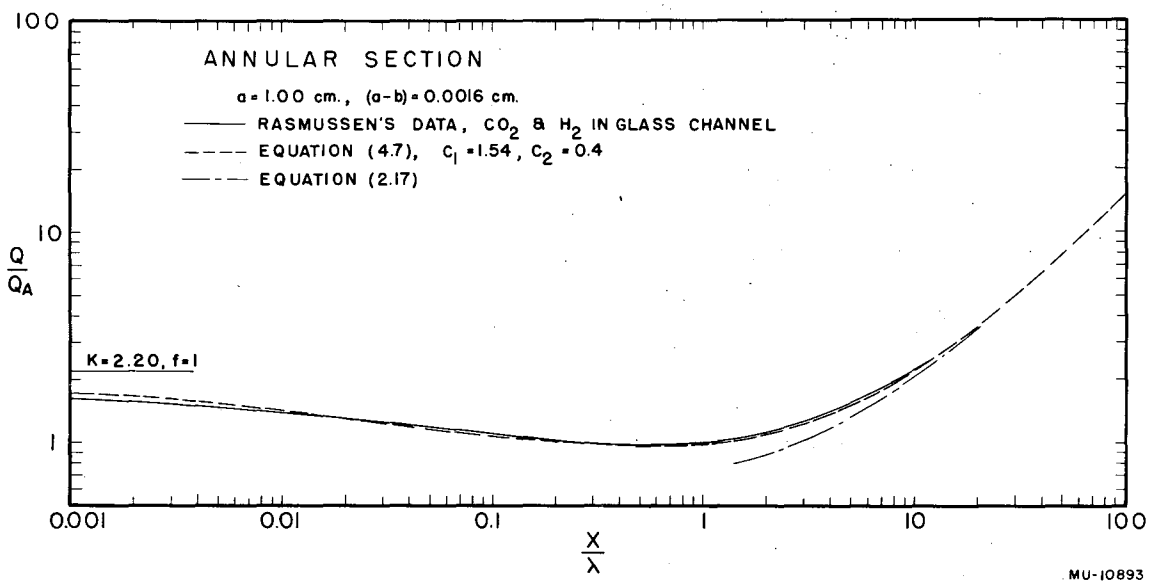

Fig. 20. Rasmussen's data of carbon dioxide and hydrogen in a glass annular channel.

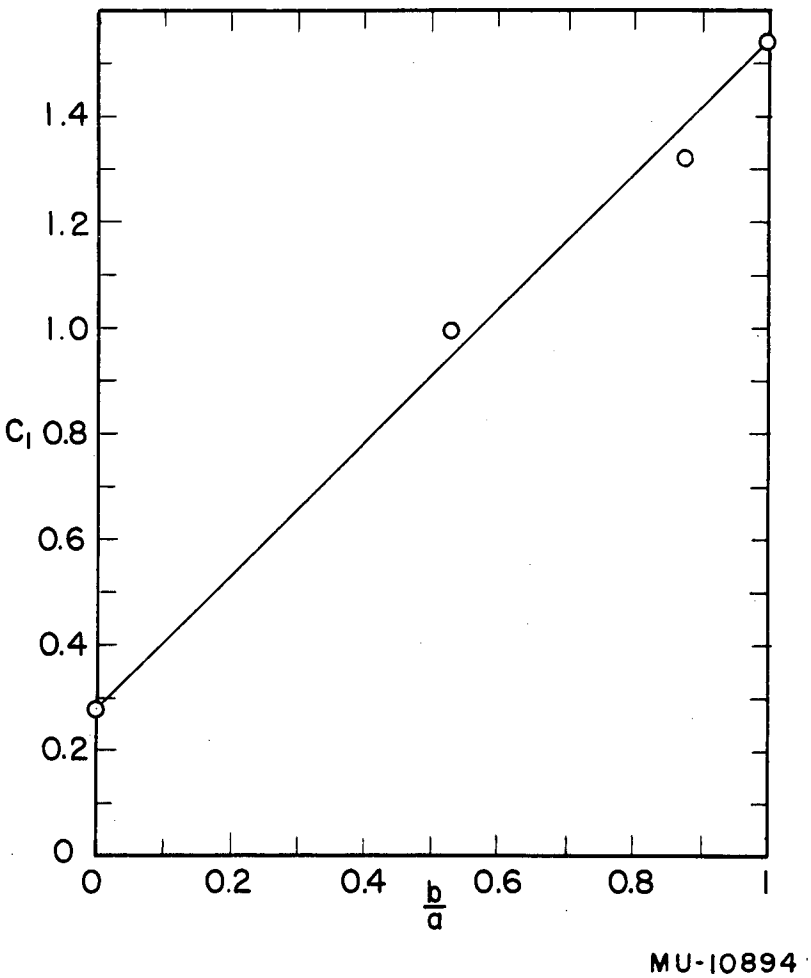

Fig. 21. Plot of C_1 as a function of $\frac{b}{a}$.

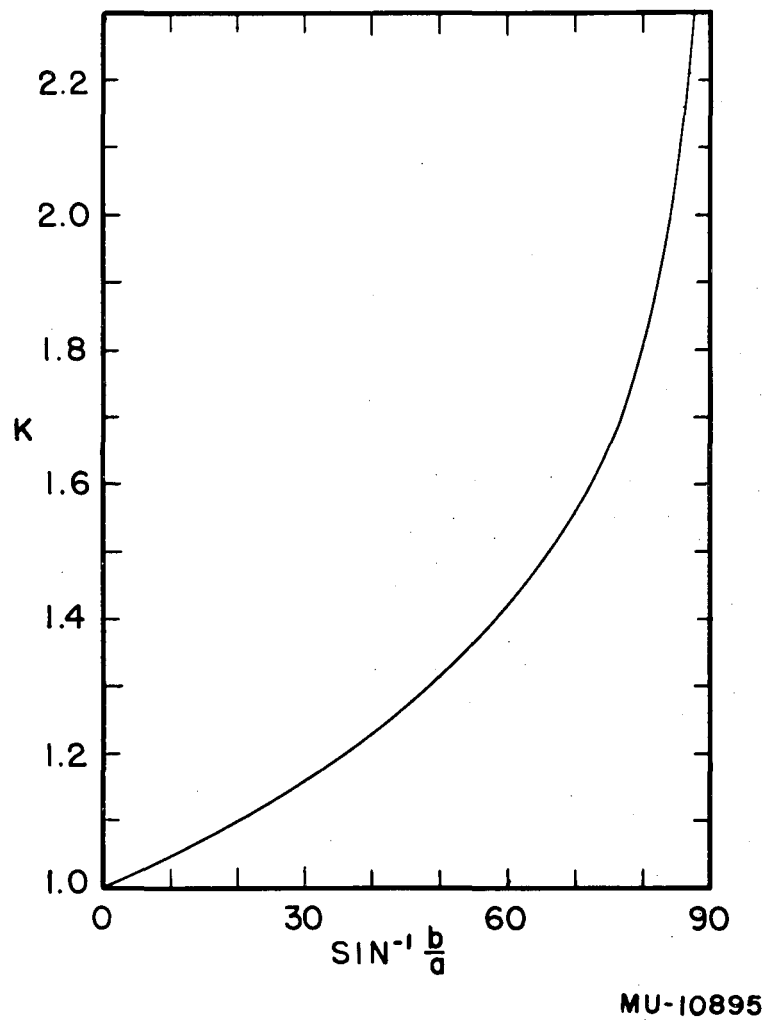

Fig. 22. Geometric factor, K, for annular sections as a function of b/a.

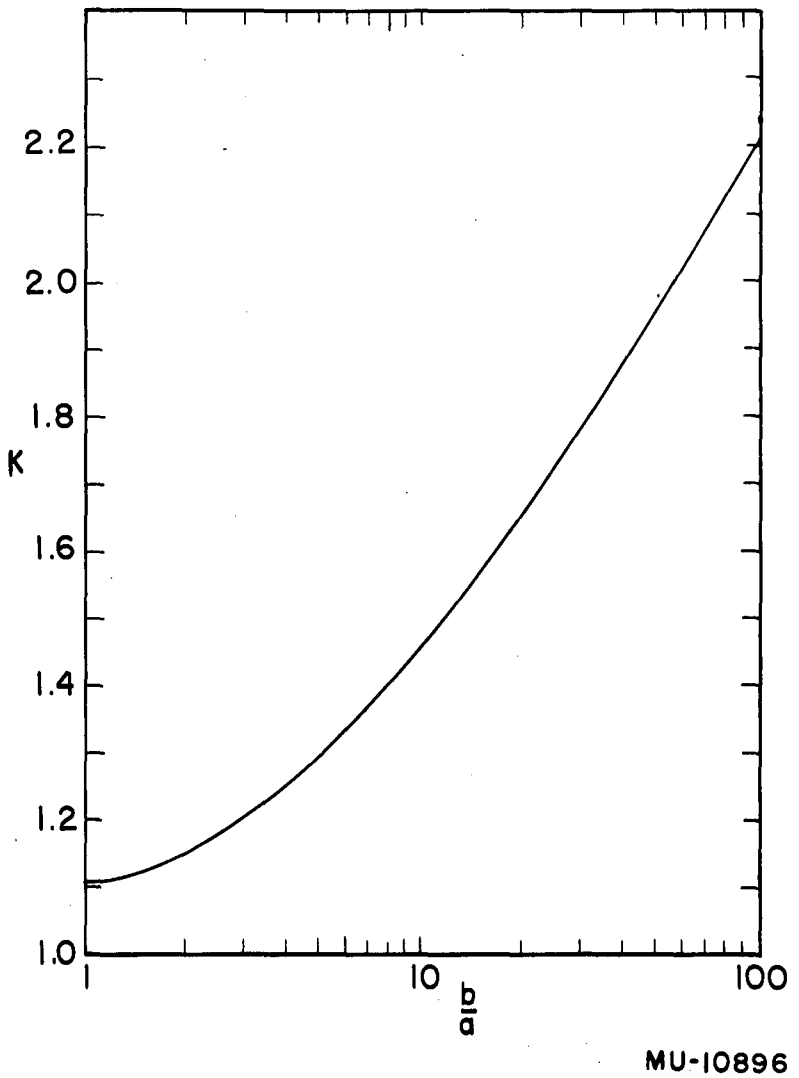

Fig. 23. Geometric factor, K, for rectangular sections as a function of $\frac{b}{a}$.

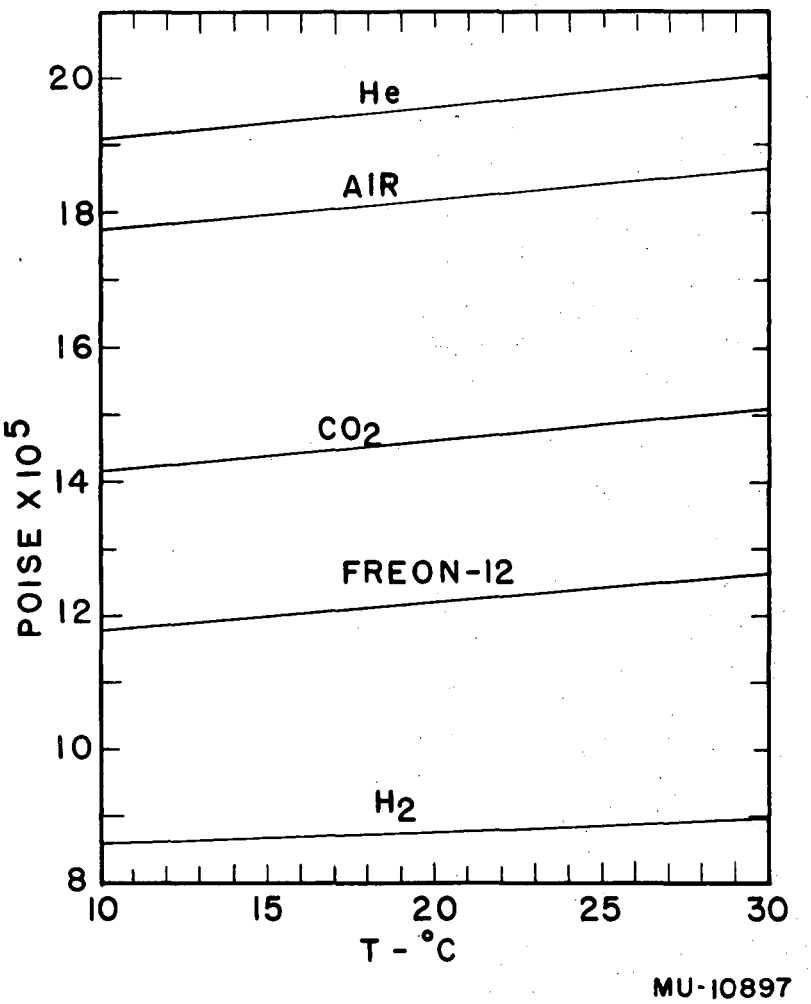

Fig. 24. Viscosity of gases as a function of temperature.

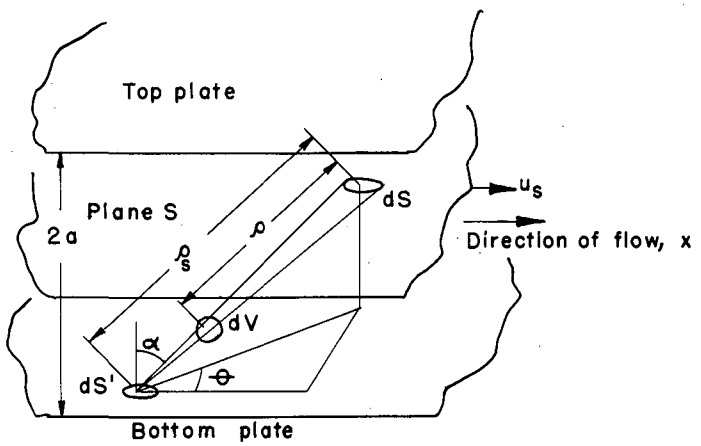
Top plate
Plane S
2a
dS
u_s
Direction of flow, x
ρ_s
ρ
dV
α
θ
dS'
Bottom plate

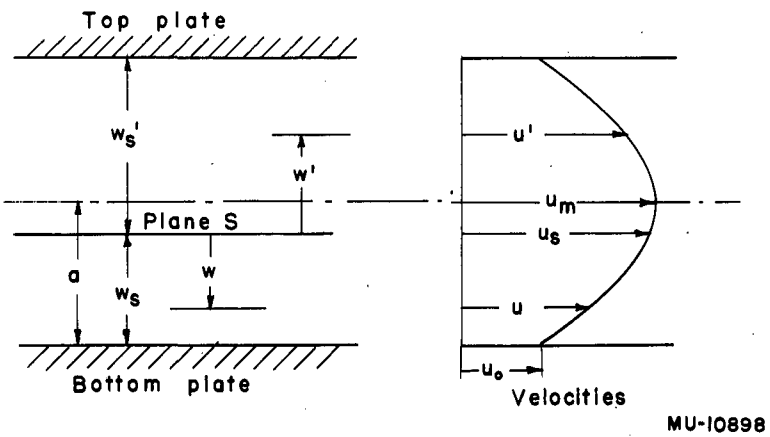
Top plate
w_s'
w'
Plane S
a
w_s
w
Bottom plate
u'
u_m
u_s
u
u_o
Velocities

MU-10898

Shear Stress Distribution between Infinite Parallel Plates in the Slip-Flow Region when the Velocity Distribution is Parabolic

Equations (2.55) and (2.58) express the rate of momentum transfer from gas and wall collisions respectively. When Eqs. (2.59), (2.61), and (2.62) are substituted into the integral form of Eq. (2.55), we get

$$M_b' = C \int_0^{2\gamma_a - \gamma_s} e^{-\gamma'/\cos\alpha} \left[2\gamma'(\gamma_a - \gamma_s) - \gamma'^2 \right] d\gamma' , \qquad (A.1)$$

where C is given by Eq. (2.64). The integration of Eq. (A.1) yields

$$M_b' = C \left[\cos\alpha(2\gamma_a\gamma_s - \gamma_s^2 + 2\cos^2\alpha + 2\gamma_a \cos\alpha)\, e^{-(2\gamma_a - \gamma_s)/\cos\alpha} + 2\cos^2\alpha(\gamma_a - \gamma_s - \cos\alpha) \right] . \qquad (A.2)$$

The corresponding expression for the momentum transfer from below, M_b, is the same as Eq. (A.2) with the exponential term, $e^{-(2\gamma_a - \gamma_s)/\cos\alpha}$, replaced by $e^{-\gamma_s/\cos\alpha}$.

The integral form of Eq. (2.58), after Eqs. (2.61) and (2.62) have been substituted, is

$$M_w' = -C \cos\alpha\, e^{-(2\gamma_a - \gamma_s)/\cos\alpha} \left[\frac{u_o}{u_m - u_o} (\gamma_a^2 + 2\gamma_a\gamma_s - \gamma_s^2) \right] . \qquad (A.3)$$

The corresponding term for M_w is again obtained by substituting $e^{-\gamma_s/\cos\alpha}$ for $e^{-(2\gamma_a - \gamma_s)/\cos\alpha}$ in Eq. (A.3).

The total rate of momentum transfer across dS is

$$M_S = M_b' + M_w' - M_b - M_w . \qquad (A.4)$$

When Eqs. (A.2), (A.3), and their counterparts are substituted into Eq. (A.4), we get

$$M_S = C \cos\alpha \left\{ \left[2\gamma_a \cos\alpha + 2\cos^2\alpha - \frac{u_o \gamma_a^2}{(u_m - u_o)} \right] \left[e^{-(2\gamma_a - \gamma_s)/\cos\alpha} - e^{-\gamma_s/\cos\alpha} \right] + 4(\gamma_a - \gamma_s) \cos^2\alpha \right\} . \quad (A.5)$$

Since we are always interested in the case in which γ_a is large, we can substitute Eq. (2.67) into Eq. (A.5):

$$M_S = B \int_0^{\frac{\pi}{2}} \cos\alpha \sin\alpha \, d\alpha \left[(2\cos^2\alpha + 2\gamma_a \cos\alpha - \frac{4}{3}\gamma_a + 1)(e^{-(2\gamma_a - \gamma_s)/\cos\alpha} - e^{-\gamma_s/\cos\alpha}) + 4\cos^2\alpha (\gamma_a - \gamma_s) \right] , \quad (A.6)$$

where

$$B = \frac{mnv}{2\gamma_a^2} (u_m - u_o) dS . \quad (A.7)$$

Let $\cos\alpha = 1/Z$, $\gamma_s' = 2\gamma_2 - \gamma_s$, (A.8)

then Eq. (A.6) becomes

$$\frac{M_S}{B} = \int_1^{\infty} \left\{ \left[\frac{2}{Z^5} + \frac{2\gamma_a}{Z^4} - \frac{1}{Z^3}\left(\frac{4}{3}\gamma_a - 1\right) \right] (e^{-\gamma_s' Z} - e^{-\gamma_s Z}) + \frac{4(\gamma_a - \gamma_s)}{Z^2} \right\} dZ . \quad (A.9)$$

We can integrate Eq. (A.9) by using the relation

$$\int_1^{\infty} \frac{e^{-\gamma_s Z}}{Z^n} = \left(\frac{1}{n-1}\right) e^{-\gamma_s} - \gamma_s \int_1^{\infty} \frac{e^{-\gamma_s Z}}{Z^{n-1}} \, dZ \quad (A.10)$$

and

$$\int_1^{\infty} \frac{e^{-\gamma_s Z}}{Z} dZ = \ln \gamma_E \gamma_S + \gamma_S - \frac{\gamma_S^2}{2!2} + \frac{\gamma_S^3}{3!3} = - E\,i\,(-\gamma_S), \quad (A.11)$$

where γ_E = Euler's constant (1.781).

The result of this integration is

$$\frac{M_S}{B} = \frac{4}{3}(\gamma_a - \gamma_S) + \left[1 - \frac{2}{3}\gamma_S' + \frac{1}{12}\gamma_S'^2 + \frac{1}{3}\gamma_a\gamma_S' - \frac{1}{12}\gamma_S'^3 + \frac{1}{3}\gamma_a\gamma_S'^2\right] e^{-\gamma_S'}$$

$$- \left[1 - \frac{2}{3}\gamma_S + \frac{1}{12}\gamma_S^2 + \frac{1}{3}\gamma_S\gamma_a - \frac{1}{12}\gamma_S^3 + \frac{1}{3}\gamma_a\gamma_S^2\right] e^{-\gamma_S}$$

$$- \gamma_S'^2 \left[\frac{\gamma_S'^2}{12} - \frac{1}{3}\gamma_a\gamma_S' + \frac{1}{2} - \frac{2}{3}\gamma_a\right] E\,i\,(-\gamma_S')$$

$$+ \gamma_S^2 \left[\frac{\gamma_S^2}{12} - \frac{1}{3}\gamma_a\gamma_S + \frac{1}{2} - \frac{2}{3}\gamma_a\right] E\,i\,(-\gamma_S) \,. \qquad (A.12)$$

For laminar flow γ_a approaches infinity; thus in the bulk of the gas γ_S also approaches infinity. The last four terms of Eq. (A.12) vanish and we have

$$\frac{M_S}{B} = \frac{4}{3}(\gamma_a - \gamma_S) \,, \qquad (A.13)$$

which satisfies Eq. (2.54). Equation (A.12) was solved for $\gamma_a = 5$ and 10 at several values of γ_S. These are given in Table II.

Experimental Errors[30]

Measured Quantities

The principal measurements made were:

1. Room and bath temperatures, T_r and T_b.

During the progress of a run the room temperature could fluctuate as much as $\pm 0.5^{\circ}C$. The bath temperature could be maintained to $\pm 0.05^{\circ}C$.

2. Barometric pressure.

The barometric pressure was measured once or twice a day and could be trusted to $\pm$ 0.5 mm of Hg. or better.

3. Upstream and downstream pressures, p_1 and p_2.

Three McLeod gauges were used to measure all vacuum pressures. A 1000-cc McLeod gauge was used to measure pressures up to 100 microns, a 700-cc gauge to measure pressures from 100 to 300 microns, and a 250-cc gauge to measure pressures above 300 microns. The accuracy of the McLeod gauges varied with pressure; therefore the probable error was computed at several pressures for the 1000-cc gauge. The mercury height in the tip could be read to $\pm$ 0.1 mm and in the leg to $\pm$ 0.25 mm at higher pressures. At lower pressures, the leg was also read to $\pm$ 0.1 mm. The probable errors at several pressures are:

Pressure--microns	0.01	0.1	1.0	10	100
Probable error--%	± 9	± 6	± 2	± 0.45	± 0.2

Pressures obtained with the 1000-cc and 700-cc McLeod gauges between 40 and 90 microns consistently agreed to within $\pm$ 0.2%. Hence the probable error of pressures obtained with the 700-cc gauge should be within $\pm$ 0.2%. The 250-cc gauge was calibrated with the 700-cc gauge to $\pm$ 0.3%. We could assign a probable error of $\pm$ 0.35% to the 250-cc gauge.

Some meniscus or capillary effect apparently existed even with tapping, especially in the 1000-cc gauge. At times the tapping made the capillary effect worse. This would increase the probable errors listed, especially at lower pressures in the 1000-cc gauge.

4. Initial, final, and running pressures in the flow meters, P_1, P_2, and P_3.

A cathetometer accurate to $\pm$ 0.05 mm was used to measure all mercury heights in the flowmeters; therefore the errors introduced to the pressures were very small, $\pm$ 0.01%. The probable errors of these pressures were within $\pm$ 0.1%.

5. Time for the pressure in the flow meter to fall from P_1 to P_2, t.

Since the cathetometer could be read quite accurately, errors in the time measurements must be attributed to human error and to sticking of the mercury. At very high and very low flow rates the reproducibility was about $\pm$ 1.0%, but in the intermediate range a greater reproducibility could be expected.

6. Physical dimensions of the apparatuses.

The tube diameters could be measured to $\pm$ 0.00025 in. These diameters were found to scatter $\pm$ 0.001 in. from the average value of several readings.

The spacing between the plates in the rectangular section was obtained by measuring the total outside thickness of the channel and subtracting the plate thicknesses. Measurements were made at 18 corresponding points along the edges and nine points along the center of the channel. The spacing, ranging from 0.1260 in. to 0.1300 in., had an average value of 0.1277 in. and a standard deviation of 0.14%.

Calculated Quantities

The following quantities were calculated:

1. X/λ, the Knudsen number.

The mean free path, λ, was calculated with the equation

$$\lambda = (2\pi RT_r/M)^{1/2} \eta/(p_1 + p_2).$$

The viscosity data are probably accurate to $\pm$ 1%. The temperature error was small. The error in $(p_1 + p_2)$ was pressure-dependent. Thus we get, for the probable error of λ as a function of $\frac{1}{2}(p_1 + p_2)$;

$(1/2)(p_1 + p_2)$ - μ	0.01	0.1	1	10	100
Probable error -- %	$\pm$9	$\pm$6.1	$\pm$2.2	$\pm$1.1	$\pm$1

For the circular and annular sections,

$$X = \frac{a^2 + b^2}{a-b} + \frac{a + b}{\ln b/a}.$$

The error in this quantity was approximately 0.2%, which is small. X equals 2a in the rectangular section. Its average value was known quite accurately. Thus, the errors in the Knudsen number are essentially those listed for λ.

2. Q/Q_A.

The flow rates were calculated from Eq. (A.20), but were corrected by the temperature ratio, T_r/T_b. Q's measured with the small flowmeter had a maximum probable error of 1.5%; with the large flowmeter, 1.1%.

Q_A was calculated with the equation

$$Q_A = \frac{8}{3} \frac{A^2}{0} (2RT/\pi M)^{\frac{1}{2}} \frac{(p_1 - p_2)}{L}.$$

At low pressures almost the entire error in Q_A was due to $(p_1 - p_2)$. The probable error in the several channels at various upstream pressures are:

Section	0.1μ	1.0μ	10μ	100μ	1000μ
Circular	±13.5%	±4.5%	±1.0%	±2.8%	-
AI	± 9.5%	±3.2%	±0.7%	±1.1%	-
AII	± 8.3%	±2.8%	±0.6%	±0.5%	±3%
Rectangular	±10.8%	±3.6%	±0.8%	±0.5%	±1.3%

Thus the approximate errors in Q/Q_A are:

Section	0.1μ	1.0μ	10μ	100μ	1000μ
Circular	±13.5%	±4.8%	±1.4%	±3%	-
AI	± 9.5%	±3.5%	±1.3%	±1.6%	-
AII	± 8.3%	±3.2%	±1.2%	±1.2%	±3.2%
Rectangular	±10.3%	±3.9%	±1.3%	±1.2%	±1.7%

Flowmeter Equations

The flow rate is given by the rate of change of the pressure-volume product in the flowmeter:

$$Q = -d(PV)/dt. \tag{A.14}$$

Since the pressure varies during the flow-rate measurement, the dependence of Q on P must be known before the integration can be carried out. This dependence is governed by the flow mechanism across the needle valve used to control the flow rate. When the mechanism of flow across the needle valve is laminar, Q is proportional to P^2; and when it is molecular, sonic, or turbulent, Q is proportional to P. In our range of operation the flow mechanism apparently changes from molecular to laminar to sonic as the flow increases, for the pressure dependence of Q with increasing flow changes from P to P^2, then back to P again.

The equation for the case in which Q is proportional to P is

$$-d(PV)/dt = C_1 P, \tag{A.15}$$

where C_1 is the meter constant. Equation (A.15) can be rearranged to give the integral form

$$\int_{P_1}^{P_2} \frac{VdP + PdV}{P} = -\int_0^t C_1 dt. \tag{A.16}$$

The volume enclosed by the meter varies with pressure owing to the change in the mercury height in the manometer leg (see Fig. 3). The variation is taken into account by the relation

$$V = V_1 - A(P_1 - P), \tag{A.17}$$

where

P = absolute pressure in the flowmeter at any time,

P_1 = absolute pressure at the start of flow measurement,

V = enclosed volume of the meter at P,

V_1 = enclosed volume of the flowmeter at P_1,

and

A = cross-section area of the manometer leg.

Substituting Eq. (A.17) into Eq. (A.16), we get

$$\int_{P_2}^{P_1} 2A\,dP + \frac{(V_1 - AP_1)}{P}\,dP = C_1 t. \qquad (A.18)$$

The integration of Eq. (A.18) yields

$$C_1 = \frac{2A(P_1 - P_2) + (V_1 - AP_1)\ln(P_1/P_2)}{t} \qquad (A.19)$$

Thus the flow rate is

$$Q = C_1 P_3 = (P_3/t)\left[2A(P_1-P_2) + (V_1-AP_1)\ln(P_1/P_2)\right] \qquad (A.20)$$

where P_3 is the pressure in the flowmeter when the pressures in the duct are being measured.

When Q is proportional to P^2, the flow equation becomes

$$d(PV)/dt = -C_2 P^2. \qquad (A.21)$$

Substituting Eq. (A.17) into Eq. (A.21) and rearranging, we get

$$\int_{P_1}^{P_2} 2A\,dP/P + (V_1 - AP_1)\,dP/P^2 = -C_2 t. \qquad (A.22)$$

The integration of Eq. (A.22) yields

$$C_2 = 2A\ln(P_1/P_2) + (V_1-AP_1)\left(\frac{1}{P_2} - \frac{1}{P_1}\right), \qquad (A.23)$$

and the flow is

$$Q = C_2 P_3^2 = \frac{P_3^2}{t}\left[2A\ln(P_1/P_2) + (V_1 - AP_1)\left(\frac{1}{P_2} - \frac{1}{P_1}\right).\right]. \qquad (A.24)$$

Normally, it is not known when the flow across the needle valve is laminar. However, it is possible to calculate the value of P_3 in terms of P_1 and P_2 so that the flow is the same when either equation is used. This is done by equating Eqs. (A.20) and (A.24), which gives us:

$$P_3 = \frac{2A(P_1 - P_2) + (V_1 - AP_1)\ln(P_1/P_2)}{2A(\ln(P_1/P_2)) + (V_1 - AP_1)(1/P_2 - 1/P_1)} . \qquad (A.25)$$

Rearranging Eq. (A.25), we get

$$P_3 = \frac{(P_1 - P_2)}{\ln \frac{P_1}{P_2}} \cdot \frac{\left[2A + (V_1 - AP_1)\frac{\ln(P_1/P_2)}{(P_1-P_2)}\right]}{\left[2A + (V_1-AP_1)\frac{(1/P_2 - 1/P_1)}{\ln(P_1/P_2)}\right]} . \qquad (A.26)$$

If P_1/P_2 is less than 1.1, which is true in our work, then we have

$$(P_1 - P_2)/\ln(P_1/P_2) \cong (P_1 + P_2)/2 \qquad (A.27)$$

and

$$\ln(P_1/P_2)/(1/P_2 - 1/P_1) \cong (P_1 + P_2)/2. \qquad (A.28)$$

Substituting Eqs. (A.27) and (A.28) into Eq. (A.26), we get

$$P_3 = (P_1 + P_2)/2. \qquad (A.29)$$

Thus, by setting the pressure in the flowmeter according to Eq. (A.29), we can use either flow equation to calculate the flow rate.

Although the term $(V_1 - AP_1)$ appeared to depend on P_1, rearrangement of the quantities will show that it is only a function of the atmospheric pressure.

Geometric Factor - K

The molecular-flow equation for infinite tube is already given in the text. The equation for molecular flow in other sections can be expressed as

$$Q_M = \frac{4}{3} \bar{v} \frac{A^2}{O} \frac{dp}{dx} K.$$

For an infinitely long annular section[11] we have

$$K = \frac{1}{(1-k)(1-k^2)} \left[1 - \frac{(1-k^2)}{2} E\right] + \frac{1}{2(1-k)} \left[F - \frac{3}{2} k\right] ,$$

where

$$E = \int_0^{\frac{\pi}{2}} (1 - k^2 \sin^2 \phi)^{1/2} \, d\phi ,$$

$$F = \int_0^{\frac{\pi}{2}} \frac{d\phi}{(1 - k^2 \sin^2 \phi)^{1/2}} ,$$

and

$$k = b/a .$$

Figure 22 shows K as a function of k.

For an infinitely long rectangular section,

$$K = \frac{3}{8} \left(\frac{a+b}{b}\right)\left(\frac{a}{b}\right)\left[\frac{b^2}{a^2} \ln \left(\frac{a}{b}\right) + 1 + \frac{a^2}{b^2}\right) + \frac{b}{a} \ln \left(\frac{b}{a} + 1 + \frac{b^2}{a^2}\right) - \frac{\left(\frac{b^2}{a^2} + 1\right)^{3/2}}{3} + \frac{\frac{b^3}{a^3} + 1}{3} \right]$$

A plot of K as a function of the aspect ratio, b/a, is shown in Fig. 23.

Physical Properties of Gases

Viscosity

The viscosities of hydrogen, carbon dioxide, and Freon-12 were obtained from Buddenburg and Wilke.[7] The viscosity of air was taken from Johnston and McClaskey.[18] The viscosity of helium was obtained from Johnston and Grilly.[19] These data are reproduced in Fig. 24.

Gas Specifications

The hydrogen used in the experiments was supplied by the University of California by an electrolytic process, 99.95% pure. Helium was supplied by the U.S. Navy, 99.99% pure. Air, of course, is drawn from the atmosphere. Carbon dioxide was supplied by Pure Carbonic, Inc., with a purity of 99.5%. Freon-12 was supplied by Kinetic Chemicals, Inc., 99.95% pure.

Physical Dimensions of Flow Channels

Circular Section:

Radius	a = 3.64 cm
Distance between pressure taps	L = 5.005 ft
Total channel length	10.5 ft

Annular Section:

Section AI

Outer radius	a = 3.64 cm
Inner radius	b = 1.905 cm
Distance between pressure taps	L = 5.005 ft
Total channel length	10.5 ft

Section AII

Inner radius	b = 3.174 cm

Other dimensions same as Section AI.

Rectangular Section:

Channel width	2b = 22.86 cm
Plate separation	2a = 0.324 cm
Distance between pressure taps	L = 24.00 in
Total channel length	50 in

Physical Dimensions of Flowmeters and McLeod Gauges

Flowmeters

The volume of the empty flowmeter is bound by the needle valve, top of the manometer leg, stopcock v_1, and the purge stopcock. The final volume depends on the amount of mercury added.

	Meter No. 1	Meter No. 2
Empty volume	1046.7 ± 1.5 cm^3	$130.40 \pm .05$ cm^3
Manometer cross section	$0.324 \pm .003$ cm^2	$0.369 \pm .001$ cm^3

McLeod Gauges

	Gauge No. 3	Gauge No. 4
Volume	693.5 cm^3	1113.8 ± 1.2 cm^3
Bore of Capillary	0.5934 cm diam	$0.14284 \pm .00005$ cm diam

Gauge No. 1 is calibrated against gauge No. 3. Its volume and bore are not known accurately.

Nomenclature

A = cross-section area of the flow channels; cross-section area of the manometer legs of the flowmeters - (L^2).

a = radius of the circular section; radius of the outer tube of the annular section; one-half the short side of the rectangular section - (L).

B = $(mnv/2\gamma_a 2)dS(u_m - u_o)$ - $(ML)/(T^2)$.

b = radius of the inner tube of the annular section; one-half of the long side of the rectangular section - (L).

C, C_1, C_2, etc. = constants of integration; correlation constants.

c = constant in viscosity equation, $\eta = cmnv\lambda$.

D_1, D_2 = geometric factors defined below Eq. (2.11).

E = $-\frac{1}{2\eta}\frac{dp}{dx}$ - $(1/TL)$.

f = fraction of molecules diffusely reflected.

K = geometric factor for molecular flow (See Appendix)

k = ratio of inner to outer radii in annular section, $\frac{b}{a}$.

L = length of channel - (L), between pressure taps.

l = liter - (L^3).

M = molecular weight; total rate of momentum transfer - (ML/T^2).

M_{Db}, M_{DW}, M_D = Momentum transfer rate due to diffusion from gas collisions, from wall collisions, and from both streams combined. - (ML/T^2).

M_S' = momentum transfer rate due to bulk flow necessary to satisfy momentum balance - (ML/T^2).

N_G = number of molecules suffering intermolecular collisions per unit time per unit duct length $(1/TL)$.

N_W = rate of collisions of molecules with the wall per unit duct length - $(1/TL)$.

n = molecular concentration - $(1/L^3)$.

O = periphery of the flow channel - (L).

P_1, P_2, P_3 = pressures in the flowmeters at the beginning of flow measurement, at the end of flow measurement, and at steady state, respectively, $(P_3 = (P_1 + P_2)/2)$ - $(\mu, M/LT^2)$.

p, p_1, p_2 = pressures in flow channel at any point, at the upstream pressure tap, and at the downstream pressure tap, respectively - $(\mu, M/LT^2)$.

Q = total mass flow rate - $(\mu\text{-}L^3/T)$.

Q_D = flow due to diffusion or self-diffusion - $(\mu\text{-}L^3)/T$.

Q_L = laminar flow rate - $(\mu\text{-}L^3)/T$.

Q_M = molecular flow rate - $(\mu\text{-}L^3)/T$.

Q_S = slip flow rate according to slip flow equation - $(\mu\text{-}L^3)/T$.

Q_S' = slip flow rate using slip velocity, u_o' - $(\mu\text{-}L^3)/T$.

Q_T = flow due to streaming of molecules after intermolecular collisions $(\mu\text{-}L^3)/T$.

q_j = the eigenvalue.

R = gas constant - $(L^2)/(^oKT^2)$.

r = radius - (L).

S = a plane between two infinite parallel plates - (L^2).

dS = an element of area in dS - (L^2).

dS' = an element of area - (L^2).

T = temperature (^oK).

t = time (T).

u = bulk velocity in channel below plane S - (L/T).

u' = bulk velocity in channel above plane S - (L/T).

u_m = maximum bulk velocity - (L/T).

u_o = velocity of slip: u_{oa} = slip velocity at the wall of the outer tube of the annular section, u_{ob} = slip velocity at the inner tube wall (L/T).

$u_{o\ avg}$ = average velocity of slip according to Eq. (2.12)-(L/T).

u_{os} = velocity of slip calculated from slip flow assumptions - (L/T).

u_o' = slip velocity at the wall necessary to give a correct momentum balance - (L/T).

$u_{o,\infty}$ = velocity of slip when $\gamma_a \longrightarrow \infty$ - (L/T).

$\bar{u}_S$ = bulk velocity at plane S - (L/T).

V = volume - (L^3).

dV = element of volume in flow channel (L^3).

v = bulk velocity in the y direction (L/T).

$\bar{v}$ = average molecular speed, $(8RT/\pi M)^{1/2}$ - (L/T).

$(\overline{v^2})^{1/2}$ = root-mean-square molecular speed $(3RT/M)^{1/2}$ - (L/T).

W,W' = distances from plane S in the lower and upper directions respectively - (L).

W_j = cosh q; b + q_j sinh $q_j b$.

w = bulk velocity in the z direction (L/T).

X = characteristic dimension of the cross section: X=a for the circular section, $X = \frac{a(1+k)Z}{(1-k^2)^2}$ for the annular section, and X = 2a for the rectangular section (L).

x = distance in the flow direction (L).

Y = a function of y.

Y = $\frac{1}{4\eta}\ \frac{dp}{dx}$ - (1/TL) [(Eqs. (2.1) through (2.10))]

y = distance from the center of a rectangular section perpendicular to the short side of the cross section - (L).

Z = the group $1-k^4 + \frac{(1-k^2)^2}{\ln k}$; also a function of z.

z = distance from the center of a rectangular section perpendicular to the long side of the cross section - (L).

Greek letters

α = the angle from the normal of a plane.

γ_E = Euler's constant, 1.781.

$\gamma, \gamma', \gamma_a, \gamma_S, \gamma_S'$ = W/λ, W'/λ, a/λ, W_S/λ, and $(2a-W)/\lambda$, respectively

ϵ = external coefficient of friction, 1/2 mnv - (M/L^2T).

ζ = coefficient of slip, 2 c λ $(\frac{2}{f} - 1)$ - (L).

η = viscosity, cmnvλ - (M/LT).

Θ = angle in a plane parallel to the flow direction measured from the direction of flow.

λ = mean free path - (L).

μ = micron (Hg).

= actual speed of a molecule (L/T).

π = 3.1416.

ρ = distance between two points in a duct (L).

τ = shear stress (M/LT^2).

= a function of y and z.

ω = solid angle.

$d\omega$ = element of solid angle subtended by dS.

References

1. H. J. Adzumi, Chem. Soc. Japan 12, 285, (1937).

2. C. R. Alancraig, "Pressure Drop for High Vacuum Flows Through Annular Sections," unpublished M.S. thesis in Chemical Engineering, University of California, Berkeley, 1951.

3. C. R., Alancraig, and L. A. Bromley, Chem. Eng. Progr. 48, 357 (1952).

4. A. S. D. Barrett, and C. H. Bosanquet, "Resistance of Ducts to Molecular Flow," Imperial Chem. Ind. Ltd. Report BR-296, Nov. 1944.

5. E. Blankenstein, Phys. Rev. 22, 582 (1923).

6. G. P. Brown, A. DiNardo, G. K. Cheng, and T. K. Sherwood, J. Appl. Phys. 17, 802 (1946).

7. J. W. Buddenburg, and C. R. Wilke, J. Phys. and Colloid Chem. 55, 1491 (1951).

8. S. Chapman, and T. G. Cowling, "The Mathematical Theory of Non-Uniform Gases," Cambridge University Press, 1939.

9. P. Clausing, Physica 9, 65 (1929).

10. P. Clausing, Ann. Physik 12, 961 (1932).

11. P. Clausing, Verd. Afd. Nat. Kon. Akad. Wet. Amst. 35, 1023 (1926).

12. R. J. Cornish, Proc. Roy. Soc. (London) A120, 691 (1928).

13. W. H. Eberhardt, "Momentum Transfer and Molecular Transport," Oak Ridge, Tenn., Report No. K-992, Physics, March 1953.

14. W. Gaede, Ann. Physik 41, 289 (1913).

15. J. W. Hiby, and M. Pahl, Z. Naturforsch. a7, 533 (1952).

16. J. W. Hiby, and M. Pahl, Z. Naturforsch. a7, 542 (1952).

17. F. C. Hurlbut, "An Experimental Molecular Beam Investigation of the Scattering of Molecules from Surfaces," Ph.D. thesis in physics, University of California, Berkeley, 1954.

References

(Page 2)

18. H. L. Johnston, and K. E. McClaskey, J. Phys. Chem. 44, 1038 (1940).

19. H. L. Johnston, and E. R. Grilly, J. Phys. Chem. 46, 948 (1948).

20. M. Knudsen, Ann. Physik 28, 75, 999 (1909).

21. A. Kundt, and E. Warburg, Pogg. Ann. 155, 337, 525 (1875).

22. H. Lamb, "Hydrodynamics," 5th ed., Cambridge University Press, London, 1924.

23. J. C. Maxwell, "Scientific Papers," N. Y. Dover Publications, Inc., p. 681.

24. R. A. Millikan, Phys. Rev. 21, 217 (1923).

25. W. C. Pollard, and R. D. Present, Phys. Rev. 73, 762 (1948).

26. R. E. H. Rasmussen, Ann. Physik 29, 665, (1937).

27. G. W. Todd, Proc. Univ. Durham Phil. Soc. 6, Pt. I, 8, (1920).

28. M. von Smoluchowski, Ann. Physik 33, 1559 (1910).

29. S. Weber, Kgl. Danske Videnskab. Selskab. Mat-fys. Medd. 28 (1954).

30. F. Daniels, et al, "Experimental Physical Chemistry," pp. 351-360, McGraw-Hill Book Co., Inc., 1949.